Wind-Induced Dynamic Behavior of Single-Skin Curtain-Wall System: A Comparative Numerical Study

Ali Bakhtiari, Aff.M.ASCE[1]; Kehinde J. Alawode[2]; Krishna Sai Vutukuru[3]; Guido Lori[4]; Amal Elawady[5]; Arindam Gan Chowdhury[6]; and Seung Jae Lee[7]

Abstract: Glass curtain walls, while broadly used as a building facade, are vulnerable to extreme winds. Curtain-wall failures in major wind events lead to substantial economic losses, and wind-induced vibration is often a major contributing factor to such failures. The main objectives of this study are to (i) present high-fidelity numerical modeling techniques to reproduce the wind-induced dynamic behavior of building facades, specifically focusing on a single-skin curtain-wall system, and (ii) highlight the impact of the interaction between facade and building structure on the wind-induced dynamic behavior of the curtain-wall system. The developed finite-element model is calibrated for a particular wind scenario tested at the Natural Hazards Engineering Research Infrastructure (NHERI) Wall of Wind Experimental Facility (WOW EF) at Florida International University (FIU), and subsequently validated to assess whether it can realistically reproduce the dynamic behavior in different scenarios involving various wind speeds and directions. This study also uncovers that the interaction between the facade and the building structure plays an important role in governing the wind-induced dynamic behavior of the curtain wall. In addition, this study finds that the presence of a vertical protrusion, attached to the facade for architectural reasons, may negatively impact the wind-induced dynamic response of the curtain wall, with this impact being influenced by the interaction between facade and structure. This study reports the significant discoveries, contributing new insights to facade design and the engineering industry. **DOI: 10.1061/JAEIED.AEENG-1725.**

Author keywords: Wind-induced dynamic behavior; Building facade; Curtain wall; Wind tunnel test; Finite-element analysis; NHERI Wall of Wind Experimental Facility.

Introduction

Glass curtain walls are broadly used as a building facade for low- to high-rise buildings (Pariafsai 2016), yet these remain the most vulnerable part during extreme wind events. The behavior of glass curtain walls under wind loads has been investigated through a quasi-static approach, highlighting the notable effect of wind on the loading and response of these structures (Gerhardt and Janser 1994; Sakhnovsky 1991). The facade industry has been conducting standardized tests using uniform static or cyclic pressures according to established testing guidelines such as ASTM E330/E330M-14 (2021), ICC TAS 202-94 (2017), EN 12155 (European Committee for Standardization 2000), and AAMA 501.1 (2005). However, since these standards focus on quasi-static responses of facade systems, these may not sufficiently cover the conditions in hurricane-prone areas, where extreme wind-induced dynamics can cause curtain-wall failures, such as pull-out and cracking (Sanders and Hargrove 2012). For example, Rizzo et al. (2021) conducted full-scale tests on a curtain-wall system measuring 5.45×7.06 m by applying uniformly distributed pressure using air jets in a quasi-static manner. The conclusion of this study highlighted that the tests had limitations in realistically assessing the facade's dynamic performance, emphasizing the necessity of more realistic full-scale wind tunnel tests.

The extensive damage to curtain walls in recent hurricanes, notably the destruction of the Capital One Tower's glass windows in Louisiana by Category 4 Hurricane Laura in 2020, underscores the critical need to significantly enhance our understanding of the wind-induced dynamic behavior of curtain-wall systems (Giusti 2020; Vutukuru et al. 2021). The curtain-wall failures related to wind-induced vibration can also negatively impact water tightness, leading to water infiltration during storm events (FEMA 488 2005). This causes significant economic losses by rendering the building unusable due to water damage to interiors and utilities although the main wind force-resisting system (MWFRS) does not suffer structural damage. Therefore, inadequate building facade performance is a significant contributor to annual hurricane-related economic losses, amounting to billions of dollars, in the coastal regions of the United States (National Science Board 2007; NCEI 2022). Furthermore, even without extreme wind conditions, wind-induced dynamics can lead to fatigue or dislodgement of hardware components, including hinges on operable parts and gaskets, resulting in failures such as entire window panels falling off.

[1]Senior Engineer, Forensics Practice, Thornton Tomasetti, Fort Lauderdale, FL 33301. ORCID: https://orcid.org/0000-0003-4286-5400. Email: abakhtiari@thorntontomasetti.com

[2]Senior Engineer, Forensics Practice, Thornton Tomasetti, Houston, TX 77024. ORCID: https://orcid.org/0000-0003-0281-7789. Email: kalawode@thorntontomasetti.com

[3]Project Lead, Forensics and Litigation, m2e Consulting Engineers, Coral Gables, FL 33134. ORCID: https://orcid.org/0000-0002-5587-5045. Email: kvutukuru@m2e.com

[4]Group Innovation and Technology, Permasteelisa S.p.A, Vittorio Veneto, Treviso 31029, Italy, Email: g.lori@permasteelisagroup.com

[5]Associate Professor, Dept. of Civil and Environmental Engineering, Florida International Univ., Miami, FL 33174. Email: aelawady@fiu.edu

[6]Professor, Dept. of Civil and Environmental Engineering, Florida International Univ., Miami, FL 33174. Email: chowdhur@fiu.edu

[7]Associate Professor, Dept. of Civil and Environmental Engineering, Florida International Univ., Miami, FL 33174 (corresponding author). ORCID: https://orcid.org/0000-0002-2180-3502. Email: sjlee@fiu.edu

Note. This manuscript was submitted on August 16, 2023; approved on June 18, 2024; published online on September 9, 2024. Discussion period open until February 9, 2025; separate discussions must be submitted for individual papers. This paper is part of the ***Journal of Architectural Engineering***, © ASCE, ISSN 1076-0431.

Nevertheless, building codes and standards do not require the examination of wind-induced dynamics for curtain-wall systems, because a building facade typically exhibits a high natural frequency and the gust energy in the wind is considered small at the high frequencies. For instance, in ASCE 7 (2022), Chapter 26, "Wind Loads: General Requirements," defines structures with their lowest natural frequencies above 1 Hz as "rigid," stating that wind-induced resonant responses for such structures are deemed insignificant and can be ignored. The ASCE 7 standard was originally developed with the dynamics of entire buildings of typical sizes in mind. Yet, in the absence of other guidance, practitioners have viewed it as also applicable to the much smaller scale of individual components and cladding (C&C) elements including curtain walls. Chapter 30, "Wind Loads: Components and Cladding," of the ASCE 7 standard specifies the requirements for determining wind pressures on C&C without inclusion of wind-induced dynamic behavior in the evaluation. Consequently, most curtain walls are designed based on static wind loads only, overlooking the dynamic effects. Recent wind tunnel studies evidenced that building envelopes can indeed experience significant resonant vibrations higher than 1 Hz. For example, wind tunnel tests conducted on roof-mounted photovoltaic (PV) systems identified a major resonant response at around 14 Hz (Estephan et al. 2022; Moravej et al. 2015). Habte et al. (2015) and Azzi et al. (2020) also reported major wind-induced resonant vibrations of standing seam metal roofs in a range of frequencies between 8 and 14 Hz. With these findings in the wind engineering community and the efforts to enhance the ASCE 7 standard, a new section "29.4.5 Ground-Mounted Fixed-Tilt Solar Panel Systems" was added to Chapter 29 in the latest version (2022). Departing from ASCE 7–16, the updated standard acknowledges the inadequacy of the 1 Hz criterion for ground-mounted solar PV systems. Yet, it still lacks guidance on the wind-induced dynamics of curtain walls.

Despite the significance, a limited number of studies have been conducted on the subject, and those that exist have employed simplistic approaches or focused on the dynamics of curtain walls subjected to seismic loads. Nakagami (2003) conducted finite-element analysis (FEA) to investigate the wind-induced vibration of a facade under a peak wind speed of 30 m/s. Two different boundary conditions were considered in the study: linear supports along the four edges; and point supports at the four corners. The linear supports resulted in a resonant response beyond 10 Hz, while the point supports led to a resonant response below 10 Hz. The study highlighted the dynamic response influenced by boundary conditions, but the potential impact of the study was limited by the absence of framing profiles in the finite-element (FE) model. Memari et al. (2021) presented a detailed FE modeling procedure of structural sealant glazing curtain-wall systems, but the major emphasis was on the dynamic response under seismic loads. The dynamic amplification factor (DAF), measuring the ratio of dynamic to static response, is commonly employed to incorporate dynamic effects into the analysis. Recent studies on DAF of curtain-wall systems, including those by Yu et al. (2017) and Alawode et al. (2023), have observed the DAF values ranging up to around 2. These findings highlight the significance of dynamic excitation in evaluating the performance of curtain walls under wind loads, emphasizing the need for deeper understanding of the wind-induced dynamics.

This study is motivated by the lack of comprehensive full-scale experimental and numerical studies to understand the wind-induced dynamic response of the curtain-wall systems. This study has two main objective: (i) present numerical modeling techniques that can realistically reproduce the wind-induced dynamic behavior of a building facade, specifically focusing on a single-skin curtain-wall system, and (ii) highlight the impact of the interaction between facade and building structure on the wind-induced dynamic behavior of the curtain wall. To this end, this study employs a set of numerical modeling techniques to develop a high-fidelity FE model. This model encompasses complex mechanical components such as double-glazing units (DGUs), operable parts, connections between frames and those between frames and glass. The developed FE single-skin curtain-wall model is calibrated for a specific wind scenario using the experiment data obtained from full-scale wind tunnel testing. The calibrated FE model is subsequently simulated to assess whether it can realistically reproduce the dynamic behavior in different scenarios involving various wind speeds and directions. Two different approaches are employed for the FE modeling to investigate the effect of facade-structure interaction: the first approach develops a "whole-structure" model, encompassing both the curtain wall and the supporting steel structure to which the curtain wall is mounted; in contrast, the second approach models the "facade-only" curtain wall as a stand-alone system, excluding the supporting structure. In addition, the study examines the influence of vertical protrusion on the dynamic response of the curtain-wall system to assess how the installation of vertical protrusion affects the facade's wind-induced dynamic behavior. The section "Wind Tunnel Test" summarizes the full-scale wind tunnel tests conducted on the single-skin curtain-wall system. The section "Numerical Modeling" discusses the modeling and calibration procedure of the developed FE curtain-wall model. The section "Analysis Results" discusses the numerical analysis results.

Wind Tunnel Test

Configuration of the Single-Skin Curtain Wall

The full-scale wind tunnel tests were conducted at the Wall of Wind Experimental Facility (WOW EF) located at Florida International University (FIU). This testing facility is one of eight Natural Hazards Engineering Research Infrastructure (NHERI) EFs supported by the US National Science Foundation (Blain et al. 2020). The WOW EF is equipped with two rows of fans, each row containing six fans (a total number of 12 fans) capable of reproducing Category 5 hurricane winds on full-scale models (Chowdhury et al. 2017). A turntable, where the full-scale model is placed, is located in front of the flow management box, allowing for testing in all wind directions (Fig. 1). Located between the fans and the experimental test section, the flow management box is designed to create atmospheric boundary layer (ABL) wind velocity profiles and turbulence characteristics for different terrain exposures. This is achieved using three triangular spires alongside an automated roughness system, facilitating the simulation of ABL and turbulence dynamics (Feng et al. 2020). The following discussion is a summary of the wind tunnel experiment that provided data for calibrating the numerical model and for comparison with the numerical analysis results. Further details on the wind tunnel experiment can be found in Alawode et al. (2023).

Fig. 2(a) shows the configuration of the single-skin curtain wall provided by Permasteelisa Group, which comprises three panels: the center panel and two side panels. The center panel houses an operable window. The single-skin curtain wall is mounted to a supporting steel structure that is bolted to the turntable underneath. Instrumentation of pressure taps requires drilling into glass panels, which is infeasible, and therefore, polycarbonate panels with the same dimensions as the facade panels are mounted on the other side of the structure to collect the pressure data. A wooden frame is attached to the supporting steel structure, and three

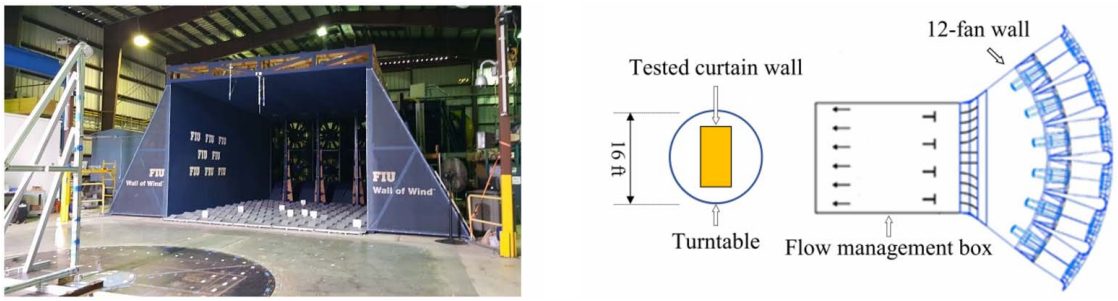

Fig. 1. FIU WOW EF: (a) interior; and (b) plan view.

Fig. 2. Tested single-skin curtain-wall structure featuring two different surfaces: (a) glass curtain-wall panels on one side; and (b) polycarbonate panels mounted on a wooden frame on the other side of the structure.

polycarbonate panels are mounted on the wooden frame, as shown in Fig. 2(b). The curtain-wall structure includes a roof on top, with an overhang of 0.41 m, and the sides are closed with wooden sidewalls as shown in the figure. While the tested model does not represent a specific floor level, the simulated ABL is representative of the conditions at a low-rise outdoor shopping plaza featuring large display windows or the first floor in a mid or high-rise building.

The effect of vertical protrusion (also broadly known as fin) on the dynamic behavior of the single-skin curtain wall is also investigated in the test. Two aluminum fins are installed on the mullions between the panels [Fig. 3(a)]. Two analog wooden fins are also designed and mounted to the polycarbonate wall side [Fig. 3(b)].

Figs. 4(a and b) show the overall dimensions, which are 3.05 m in height and 3.65 m in width (10 × 12 ft). The curtain-wall unit features a typical floor-to-floor height that is representative of standard building measurements. The operable window's height is 1.87 m, and its width is 0.6 m (6.13 × 1.96 ft). The supporting steel structure, to which the curtain wall is mounted, has rectangular dimensions of 3.05 m in height, 2.76 m in width, and 1.8 m in depth (10 × 9 × 5.9 ft). The wooden sidewalls have a thickness of 15 cm. The 4.00 × 2.62 m wooden roof has a thickness of 8 cm. The curtain wall includes five vertical joints (denoted by J#) as shown in Figs. 4(a and b). Fig. 4(c) shows an enlarged image of the cross section for Joint 2 (J2) as an example, illustrating the anatomy of the connection. In this connection, the glass is affixed to the mullion (a vertical framing element of a curtain-wall system) using structural silicone.

Sensor Instrumentation and Test Protocol

A total number of 110 pressure taps are instrumented on the polycarbonate panels, with two additional taps instrumented inside the model. Additional 16 taps are instrumented on the vertical protrusion. A total of 12 strain gauges are installed behind the mullions (with their locations shown as S# in Fig. 5) of the glass curtain-wall panels, while five accelerometers are placed on the glass. The locations of five accelerometers are shown as A# in the figure. Therefore, pressure data are obtained from the polycarbonate panels, while acceleration and strain data are obtained from the glass curtain-wall panels and the mullions.

The sampling frequency for pressure measurements is 512 Hz. Pressure data are obtained at the wind speed of 22.35 m/s (50 mph) and wind direction is varied from 0° (normal direction to the polycarbonate panels) to 180° by rotating the turntable in 15° increments (Fig. 6). The collected pressure data are postprocessed, where a tubing transfer function is applied to correct for any distortions caused by tubing length (Irwin et al. 1979). The acceleration and strain data are obtained at wind speeds of 22.35, 31.30, and 40.23 m/s. Wind directions vary from 0° to 315° in 45° increments. The test duration is 10 min for 22.35 m/s, and 5 min for 31.30 and 40.23 m/s, respectively. With the

(a) (b)

Fig. 3. Curtain wall with vertical protrusion: (a) glass curtain-wall panels; and (b) polycarbonate panels.

possibility of permanent deformation, the shorter test duration of 5 min is considered for the higher wind speeds. The protocol of the wind tunnel tests is summarized in Table 1.

The mean wind speed (U_{ref}) at the reference height (Z_{ref}), which is the roof level at 3.2 m, is measured as 21.97 m/s for the 22.35 m/s wind. A roughness length z_0 of 0.08 m represents an open terrain ABL simulation for the wind tunnel tests. The wind speed and turbulence characteristics are measured along the center of the turntable using Cobra probes instruments. The mean wind speed and turbulence intensity profiles obtained at the turntable center are shown in Fig. 7. The comparison with the ESDU item 85020 (ESDU 2001) indicates that the simulated wind mirrors the characteristics of the ABL wind. The turbulence intensity I_u at the roof height is 5%. The simulated wind profile adheres closely to a logarithmic shape, which is particularly relevant for low-rise building units, providing a realistic representation of the wind exposure these structures are subjected to. Additional insights into the flow characteristics from full-scale wind tunnel experiments, including peaks, fluctuations, spatial variations, and coherence on the curtain wall under various wind directions, are elaborated in the companion articles that focus on the experimental aspect for this research (Alawode 2023; Alawode et al. 2023).

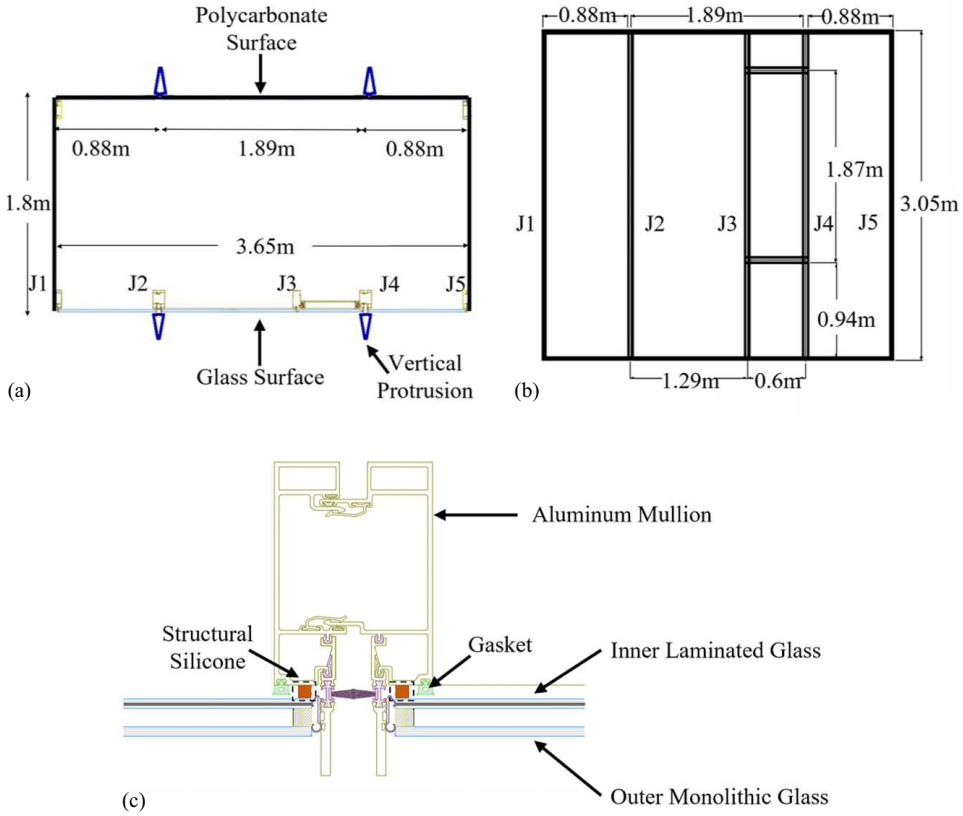

Fig. 4. The overall dimension of the tested single-skin curtain wall, where J# refers to a vertical joint number: (a) plan view (shown with vertical protrusion); (b) elevation view; and (c) cross section of J2.

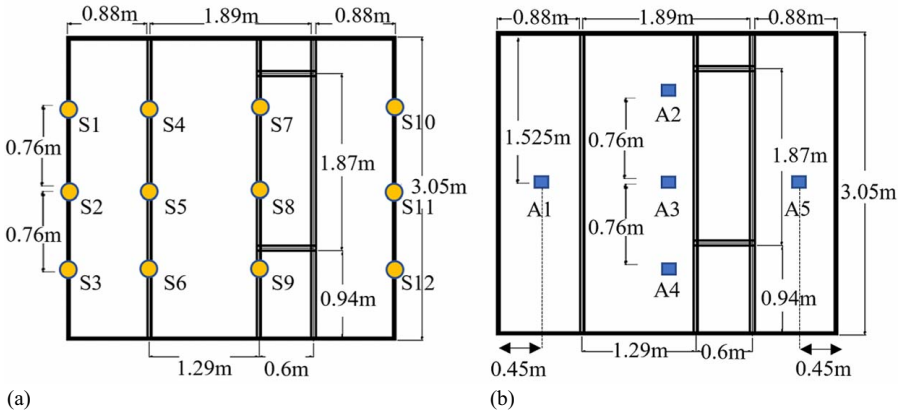

Fig. 5. Sensor locations on the glass curtain-wall side: (a) strain gauges; and (b) accelerometers.

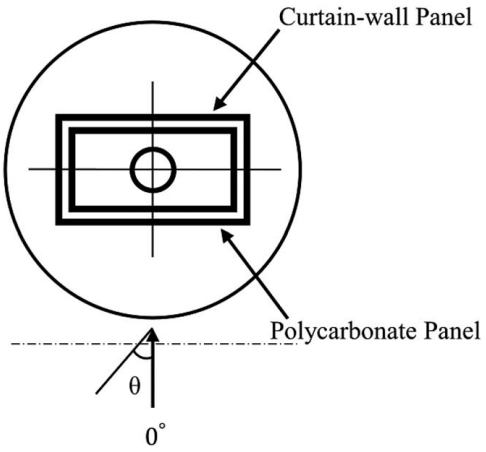

Fig. 6. Wind direction (plan view).

The data acquisition in the experiment is not performed simultaneously, as the pressure and acceleration data are obtained separately with a 180° difference. For example, pressure data for the normal wind direction (i.e., 0°) is obtained from the polycarbonate panels, whereas the acceleration and strain data for the same normal direction is obtained at 180° from the glass curtain-wall panels (Fig. 6). This arrangement in the experiment may potentially cause confusion for readers since both 0° and 180° can be viewed as normal wind directions depending on the type of data obtained. Therefore, to ensure clarity in the numerical modeling discussed in the subsequent sections, the wind direction will be designated based on the polycarbonate side. For example, the normal wind direction will be simply referred to as 0°.

Table 1. Testing protocol

Data obtained	Wind speed	Wind direction θ (degree)	Test duration (minutes)
Pressure	22.35 m/s (50 mph)	0–180 (in 15-degree increments)	1
Acceleration and strain	22.35 m/s (50 mph)	0–315 (in 45-degree increments)	10
	31.30 m/s (70 mph)	0–315 (in 45-degree increments)	5
	40.23 m/s (90 mph)	0–315 (in 45-degree increments)	5

Numerical Modeling

Single-Skin Curtain Wall

An FE model of the single-skin curtain-wall system is developed to reproduce the characteristics of wind-induced vibrations observed in the full-scale tests at the WOW EF. This study is aligned with the industry needs by developing strategies for high-fidelity

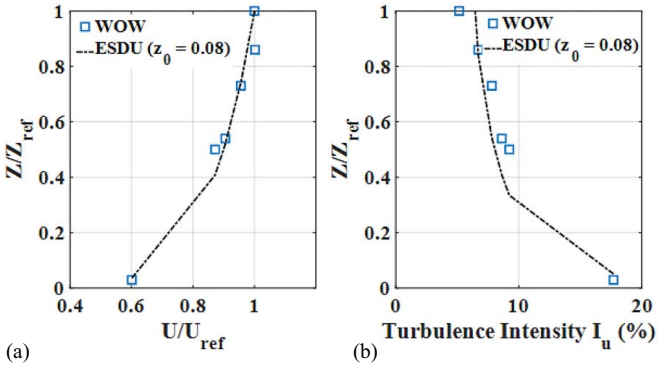

Fig. 7. Comparison of WOW data with ESDU: (a) mean wind speed profile; and (b) turbulence intensity profiles. (Reprinted from Alawode et al. 2023, © ASCE.)

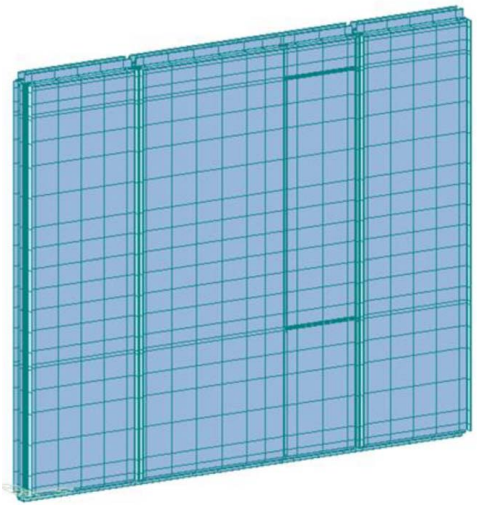

Fig. 8. Developed FE model of the single-skin curtain wall.

numerical modeling suitable for adoption by the facade industry. For this effort, Midas Gen, a commercial FEA software, is utilized for the FE modeling (Midas Information Technology 2021). Fig. 8 shows the developed FE curtain-wall model. The curtain-wall model is composed of frames and glass, which are assembled by mechanical fixings and structural silicone (wet glazing).

a. *Modeling frames*: Beam elements with 6 degrees of freedom (DOFs) per node (12 DOFs in total) are used for modeling (i) the main frame and (ii) the sash/window frame for the operable part as shown in Fig. 9. Employing 3D solid elements, such as 8-node or higher-order hexahedral brick elements, for modeling the detailed geometry of complex framing profiles could improve accuracy. However, the higher computational costs associated with these solid elements can make calibration and parametric studies excessively expensive. Given that the FEAs in the facade industry are typically conducted on ordinary personal computers with limited computing power, this approach utilizing beam elements ensures a balance between simulation fidelity and computational cost. The main frame includes mullions and transoms that are vertical and horizontal framing elements, respectively. The operable part is mounted to the main frame in the designated location as shown in Fig. 9. While the operable part can be opened – separating the sash from the window frames – this study only considers the closed condition, as it is typical during high-wind events. The curtain-wall system features nine different framing profiles, as shown in Fig. 10(a), which are considered for the numerical modeling. The cross-sectional properties of each profile including area

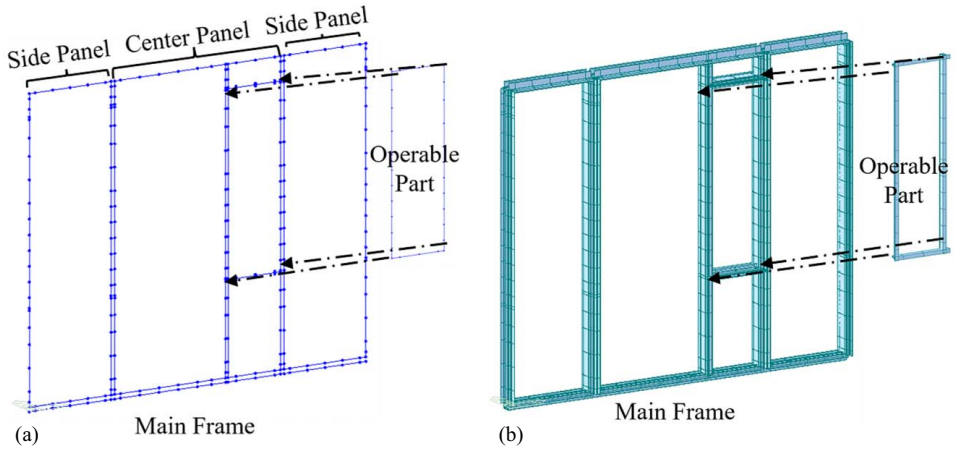

Fig. 9. The modeled main frame (mullions and transoms) and sash/window frame for the operable part: (a) the frames are modeled using 12-DOF beam elements; and (b) 3D visualization featuring the modeled framing profiles.

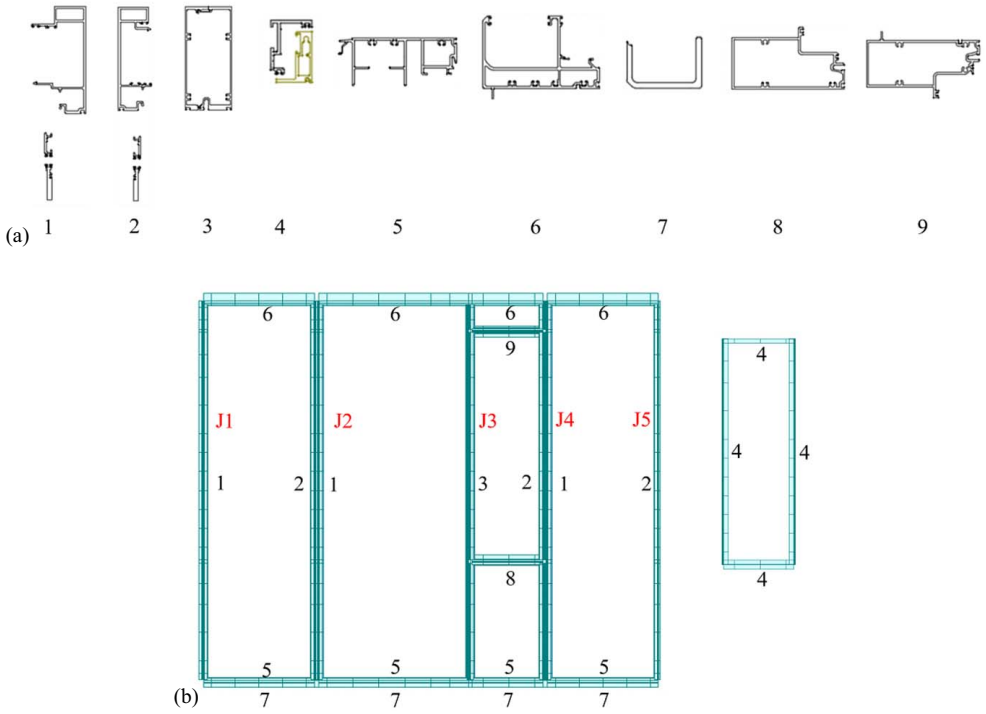

Fig. 10. Framing profiles: (a) cross sections of the nine framing profiles; profile #4 consists of both sash and window frames of the operable part, where the sash frame is presented in a brighter color; and (b) location of the framing profiles.

and second moments of area (I_{XX}, I_{YY}, and I_{XY}) are presented in Table 2, which are computed using CAD software. In calculating the second moment of area of profiles #1 and #2, the composite action of the separate parts is also considered. The geometric properties are incorporated into the modeling of the FE beam elements representing the frames.

b. *Modeling connections between the frames*: The mullion and transom in each panel are joined by a shared node; for example, framing profiles #1 and #6 are adjoined at the upper left corner in Fig. 10(b). A set of elastic links is employed to model the connection of two frames placed in parallel, reproducing the mechanical coupling between them. The elastic link has 6 DOFs with translational and rotational stiffnesses to all local *x*-, *y*-, and *z*-directions. Fig. 11 illustrates an example of assembling two mullion frames next to each other (framing profiles #2 and #1 at J2 in Fig. 10) using the 6-DOF elastic links. The same approach is used to model the intermediate mullion (profile #3) composed of two parts. The interaction between the main and sash/window frames (profiles #2, #3, #8, #9, and profile #4) is also modeled using the 6-DOF elastic links to mount the operable part to the main frame.

c. *Modeling glass*: Glass modeling is of great importance due to its extensive coverage in the curtain-wall surface and its mass, playing a substantial role in governing the overall dynamic response of the system. Therefore, the glass properties including mass and stiffness need to be properly modeled to realistically reproduce the dynamic behavior. However, glass modeling is not often straightforward if multiple layers are used, as in insulated laminated glass, which is the case with the tested curtain-wall system in this study. The glass used in the curtain wall is a DGU, and its schematic drawing is shown in Fig. 12. The DGU is composed of inner and outer glass layers with a gap that is maintained by a thermal spacer. The outer glass is a monolithic glass while the inner glass is a laminated glass where a polyvinyl butyral (PVB) interlayer is between the two layers of monolithic glass. Therefore, to numerically model it with a plate element, an equivalent glass thickness needs to be estimated to represent the properties of the DGU. Fig. 13 summarizes the estimated equivalent properties for the five different types of DGU used in the curtain wall. The hatching code indicates the location of each glass. The effective thickness of the (inner) laminated glass is first estimated using the method by Galuppi and Royer-Carfagni (2012), which is shown in the fifth column of the figure. The approach discussed in the European Standard EN 16612 (European Committee for Standardization 2019) is then adopted to back-calculate the overall effective stiffness of the DGU and subsequently the equivalent thickness. The thickness ratio, denoted as *R*, is calculated by comparing the equivalent DGU thickness to the sum of both the outer and the equivalent inner layers. The estimated equivalent DGU is thinner compared with the original. To compensate for this difference in thickness, the unit weight of the glass is increased to match the mass of the original DGU. This approach effectively models the stiffness and mass properties of the DGU, enabling the realistic reproduction of the facade's dynamic behavior. In glass modeling, 4-node plate elements are used. The initial placement of nodes is based on the locations of pressure taps on the

Table 2. Cross-sectional properties of the framing profiles

#	Framing profile	Area (mm^2)	I_{XX} (mm^4)	I_{YY} (mm^4)	I_{XY} (mm^4)
1	Left mullion	1,652	3.77×10^6	5.53×10^5	1.93×10^5
2	Right mullion	1,587	3.64×10^6	2.84×10^5	1.74×10^5
3	Intermediate mullion	1,619	5.39×10^6	2.59×10^5	2.36×10^5
4	Operable part	445	1.42×10^5	3.04×10^4	2.78×10^4
5	Bottom transom	1,329	2.76×10^6	4.00×10^5	4.49×10^4
6	Top transom	1,729	3.77×10^6	1.21×10^6	3.10×10^5
7	C-shape beam	1,187	1.40×10^6	3.66×10^5	5.54×10^4
8	Intermediate bottom transom	1,355	3.53×10^6	1.05×10^6	2.56×10^5
9	Intermediate top transom	1,355	3.54×10^6	8.95×10^5	1.91×10^5

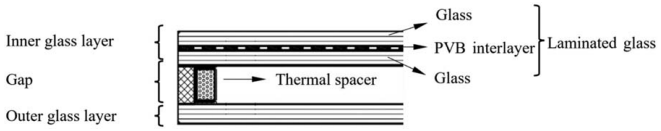

Fig. 12. Schematic drawing of the DGU.

	Outer glass layer (mm)	Gap (mm)	Inner glass layer (with PVB) (mm)	Equivalent inner layer thickness (mm)	Equivalent DGU thickness (mm)	Thickness ratio (R)	Scaled unit weight (kg/m^3)
	6.35	12.70	10.29	9.75	**10.40**	0.65	3430
	4.76	15.88	4.76	4.76	**5.73**	0.60	3678
	6.35	12.70	10.29	9.27	**9.53**	0.61	3628
	6.35	12.70	10.29	9.07	**8.87**	0.58	3845
	10.00	12.00	6.00	6.00	**10.72**	0.67	3322

Fig. 13. Computed equivalent DGU thicknesses.

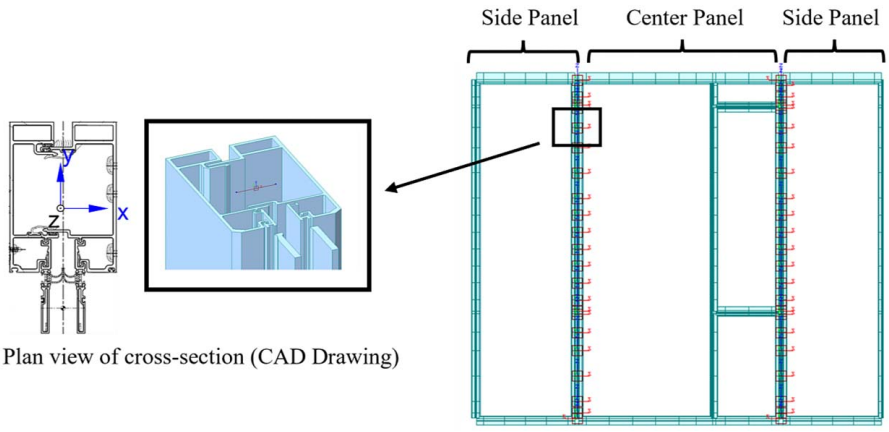

Fig. 11. Modeling connection between the neighboring panels, where 6-DOF elastic links are used.

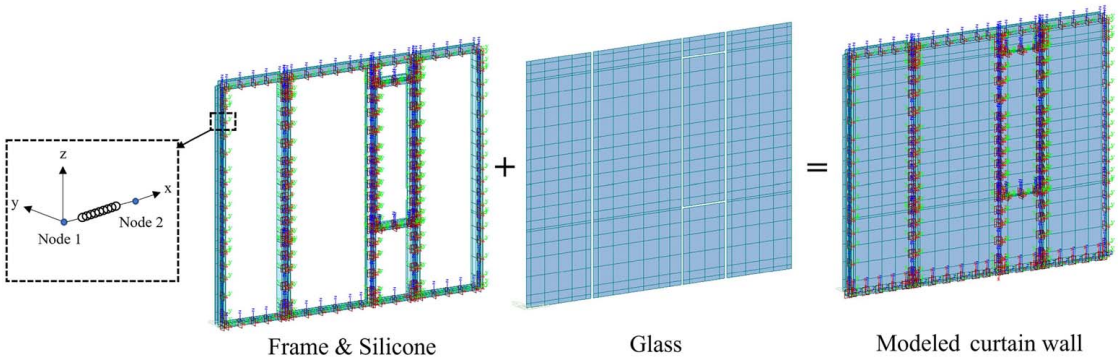

Fig. 14. Modeled curtain wall features glass and frames joined by structural silicone, represented by elastic links illustrated in the inset image.

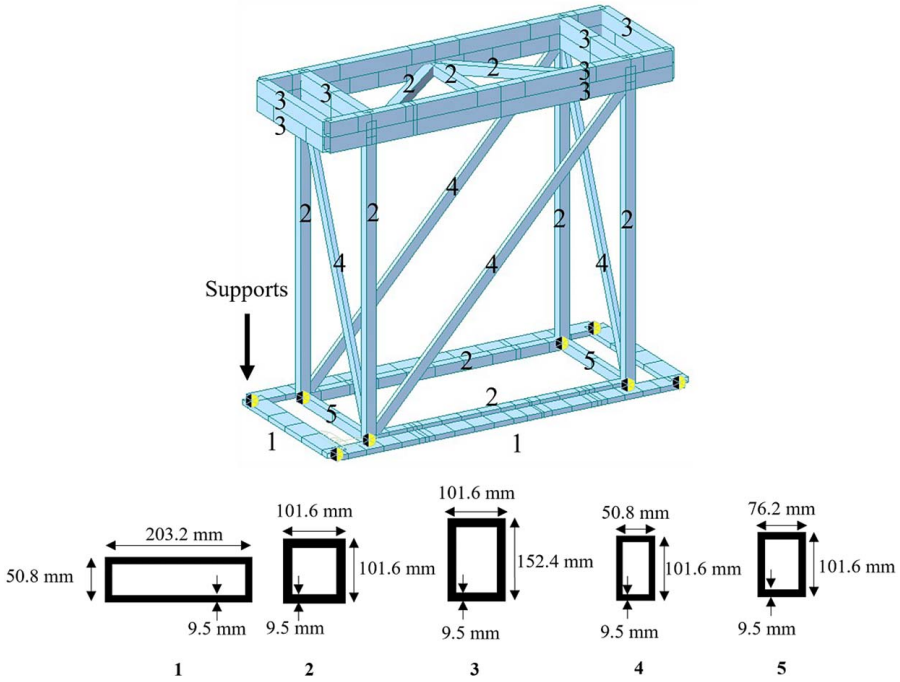

Fig. 15. FE model of the supporting steel structure, with its bolted connections to the turntable highlighted as "supports" using half-colored hexagon icons the five framing profiles shown in the figure are used to fabricate the steel structure.

glass, as identified in wind tunnel experiments. Mesh density is subsequently enhanced, with the initial nodes remaining fixed, until further enhancement would not warrant significant improvement in simulation fidelity.

d. *Assembling frames and glass*: Structural silicone assembles the glass and frames in the tested curtain-wall system. In this study, the 6-DOF elastic links are used to numerically represent the silicone. Fig. 14 shows the modeled curtain wall with elastic links assembling the glass and frames.

Table 3. Cross-sectional properties of the framing profiles of the supporting steel structure

Framing profile #	Area (mm^2)	I_{XX} (mm^4)	I_{YY} (mm^4)	I_{XY} (mm^4)
1	4,470	1.72×10^6	1.89×10^7	5.17×10^6
2	3,503	5.00×10^6	5.00×10^6	7.43×10^6
3	4,470	1.36×10^7	7.06×10^6	1.40×10^7
4	2,542	2.95×10^6	8.89×10^5	2.06×10^6
5	3,026	3.98×10^6	2.45×10^6	4.52×10^6

Whole-Structure Model

The full-scale curtain-wall system tested at the WOW EF is composed of the supporting steel structure, polycarbonate panels,

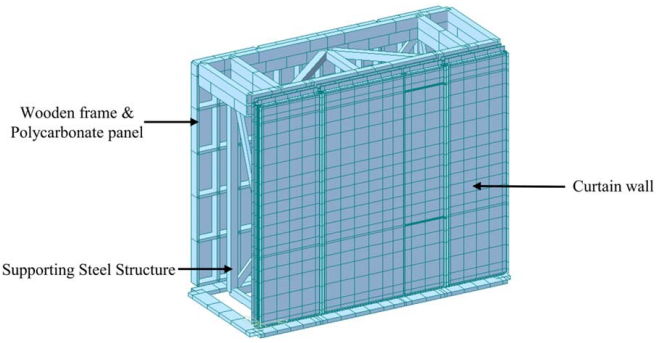

Fig. 16. The glass curtain-wall panels (front) and the polycarbonate panels (rear) attached to the supporting steel structure.

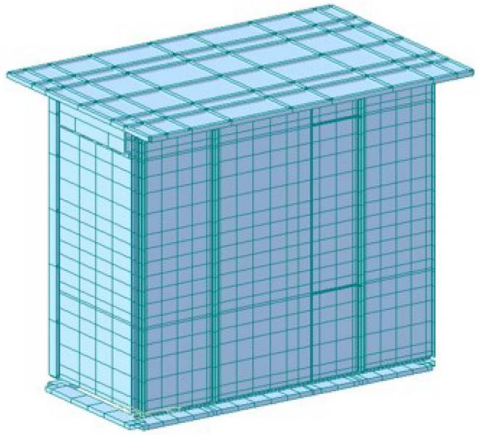

Fig. 17. The FE "whole-structure" model including the supporting steel structure, curtain-wall panels, polycarbonate panels, side walls, and roof.

sidewalls, and roof as well as the single-skin glass curtain wall. Therefore, the development of the "whole-structure" model would enable a fair comparison between the experiment data and the FE analysis results. Fig. 15 shows the developed FE model of the supporting steel structure including the main steel structure connected to perimeter beams at the bottom. The perimeter beams are bolted to the turntable in the experiment, which are numerically modeled with supports in the FE model as shown in the figure. The 12-DOF beam elements are utilized to model the beams and columns of the supporting steel structure. Fig. 15 also shows the geometries of the framing profiles used to fabricate the steel structure. Table 3 presents the cross-sectional properties of the profiles. The developed single-skin curtain-wall model (Fig. 8) is then mounted to the front side of the supporting

Table 4. Material properties used in the FE model

Material	Modulus, E (MPa)	Poisson ratio, ν	Density, ρ (kg/m^3)
Aluminum	70,940	0.33	2,768
Steel	200,000	0.30	7,861
Wood	4,000	0.31	830
Polycarbonate	1,793	0.31	1,190

Table 5. Calibrated values for the modeled connections and silicones

Item # in Fig. 18	Connections and silicones	Axial stiffness (kN/m)	Shear stiffness (kN/m)	Rotational stiffness (kN·m/rad)
1	Curtain wall's top connection to the steel structure	17,513	17,513	11.29
2	Curtain wall's bottom connection to the structure	5,254	5,254	3.38
3	Steel structure's supports	7,005	7,005	4.52
4	Intermullion connection	700	700	0.45
5	Center panel's silicone	175	175	0.11
6	Side panel's silicone	166	166	0.10

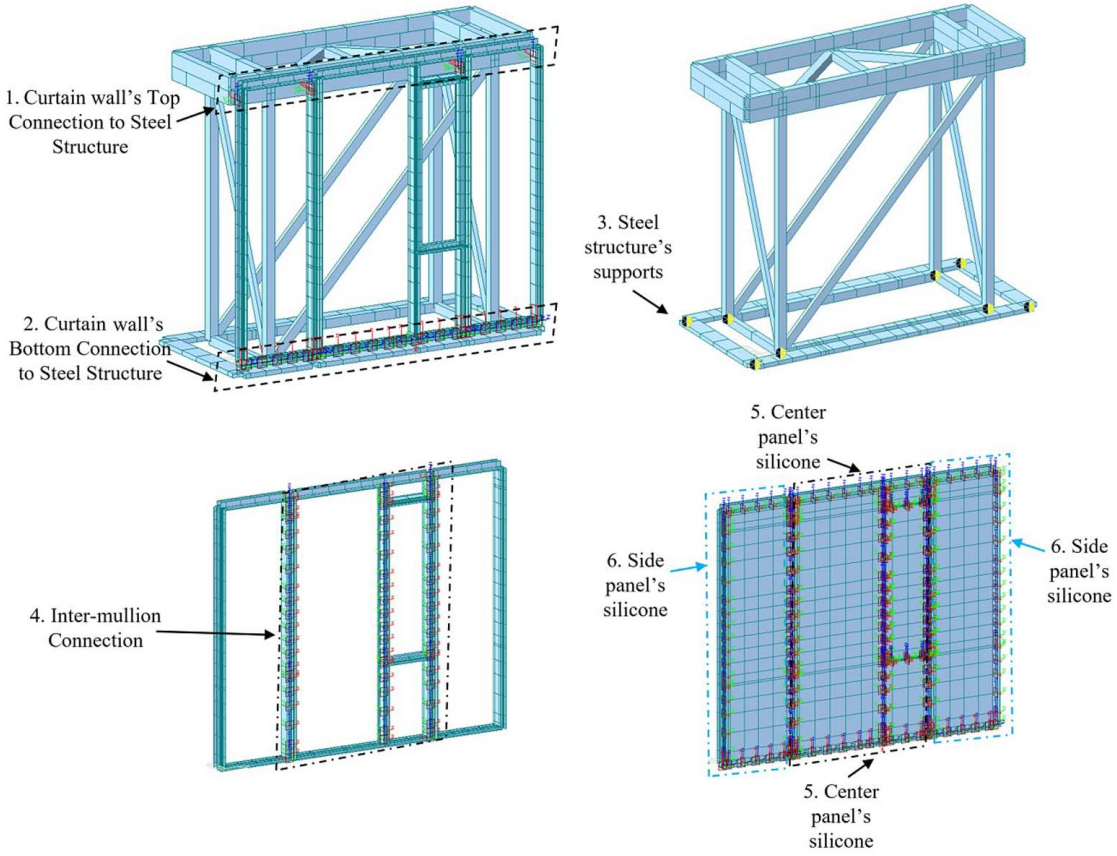

Fig. 18. Connections and silicones in the FE model.

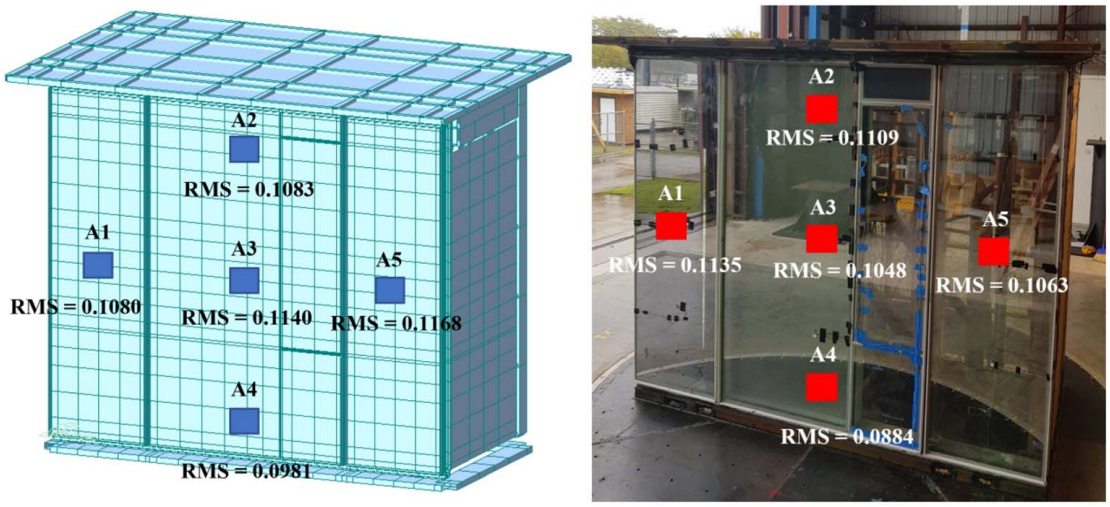

(a) (b)

Fig. 19. RMS values of acceleration time history (m/s^2) for 22.35 m/s and 0° wind: (a) whole-structure FE model; and (b) experiment data.

structure as shown in Fig. 16. The wooden frame and polycarbonate panel models are also developed and connected to the rear side of the supporting structure. The developed whole-structure model with the wooden sidewalls and roof is shown in Fig. 17. The material properties used in modeling the whole structure are summarized in Table 4.

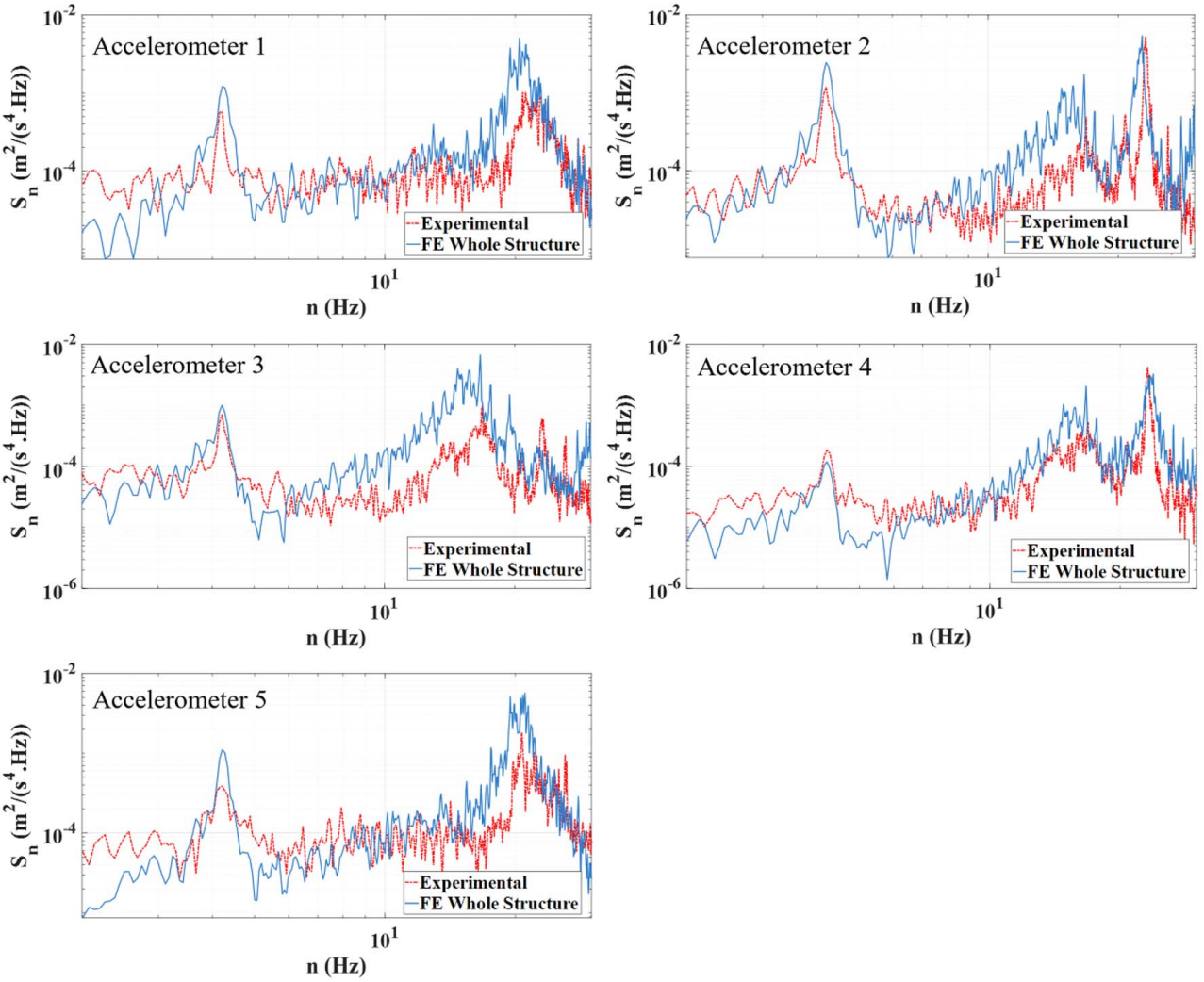

Fig. 20. Acceleration PSDs of the whole-structure FE model compared with the experiment data for 22.35 m/s and 0° wind.

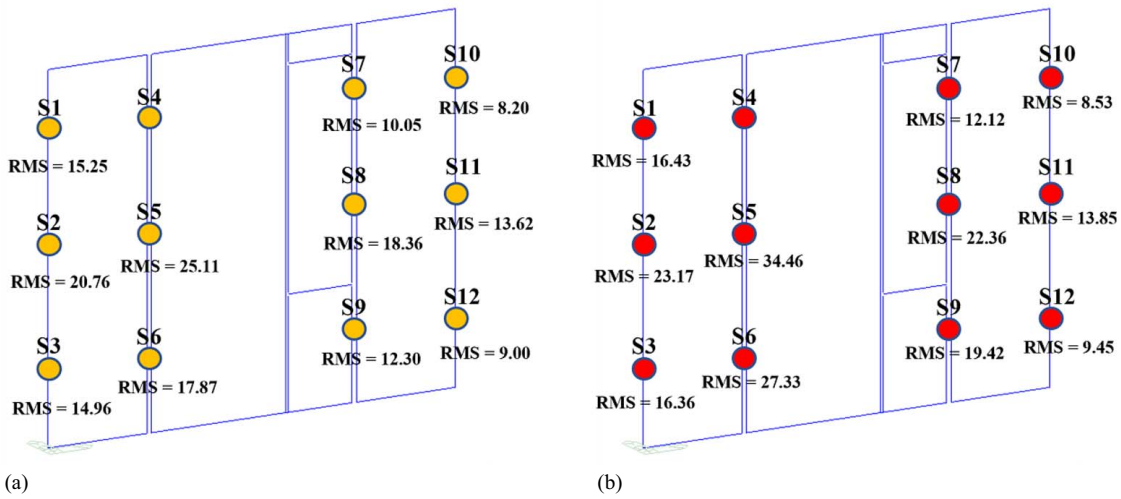

Fig. 21. RMS values of strain time history (shown in $\mu\varepsilon$) for 22.35 m/s and 0° wind: (a) whole-structure FE model; and (b) experiment data.

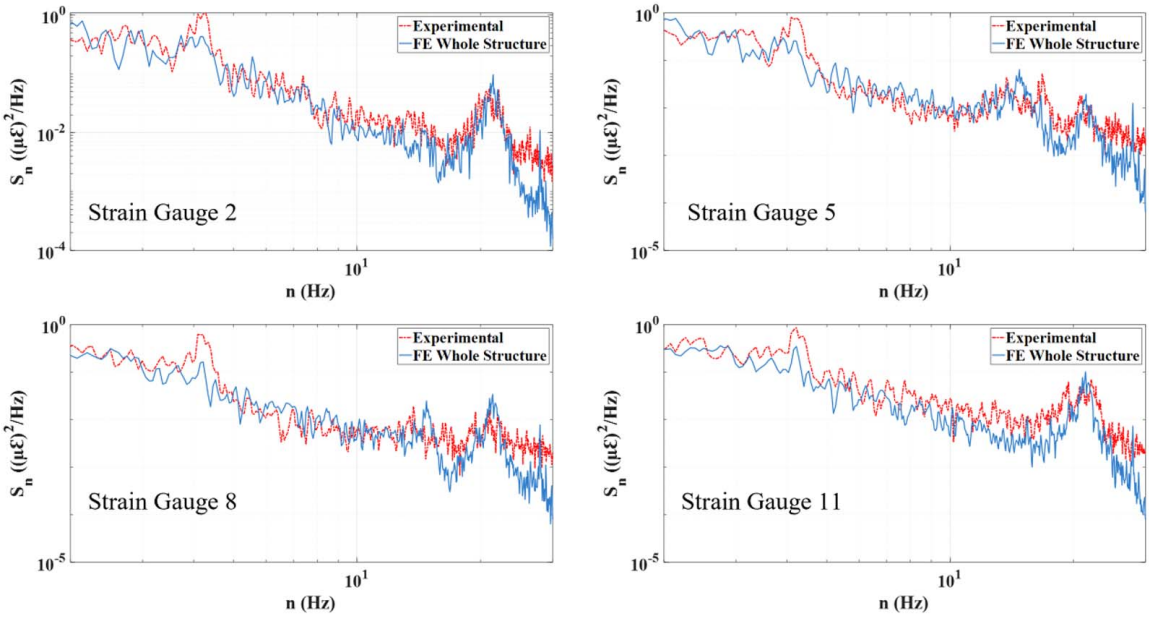

Fig. 22. Strain PSDs of the whole-structure FE model compared with the experiment data for 22.35 m/s and 0° wind.

Calibration

The pressure time history data, collected from the pressure taps in the wind tunnel test, are utilized to model the wind load. This modeling employs the data corresponding to a wind speed of 22.35 m/s and a wind direction normal (0°) to the curtain-wall surface. The raw data are expressed in terms of the pressure coefficient, denoted as C_p. Midas Gen FEA software requires nodal load time history as input for dynamic analysis. Therefore, the C_p time histories are first converted to pressure time histories using

$$p(t) = 1/2 \times \rho_{\text{air}} \times C_p \times U_{\text{ref}}^2 \tag{1}$$

where $p(t)$ = pressure time history; ρ_{air} = air density; C_p = pressure coefficient; and U_{ref} = reference wind speed measured at the roof level during the wind tunnel test.

The C_p time histories are then converted to nodal load time histories by considering the tributary area of each node using

$$F_i(t) = p_i(t) \times A_i \tag{2}$$

where $F_i(t)$ = wind load at node i at time t; $p_i(t)$ = interpolated pressure; and A_i = tributary area of the node i.

Table 6. RMS values of acceleration time history (m/s^2) of the whole-structure FE model, compared with the experiment data for 31.30 m/s and 0° wind

Accelerometer #	FE analysis (m/s^2)	Experiment data (m/s^2)	Difference (%)
1	0.4489	0.4925	8.9
2	0.3186	0.3304	3.6
3	0.3400	0.3200	6.2
4	0.3240	0.3162	2.5
5	0.4798	0.5486	12.6

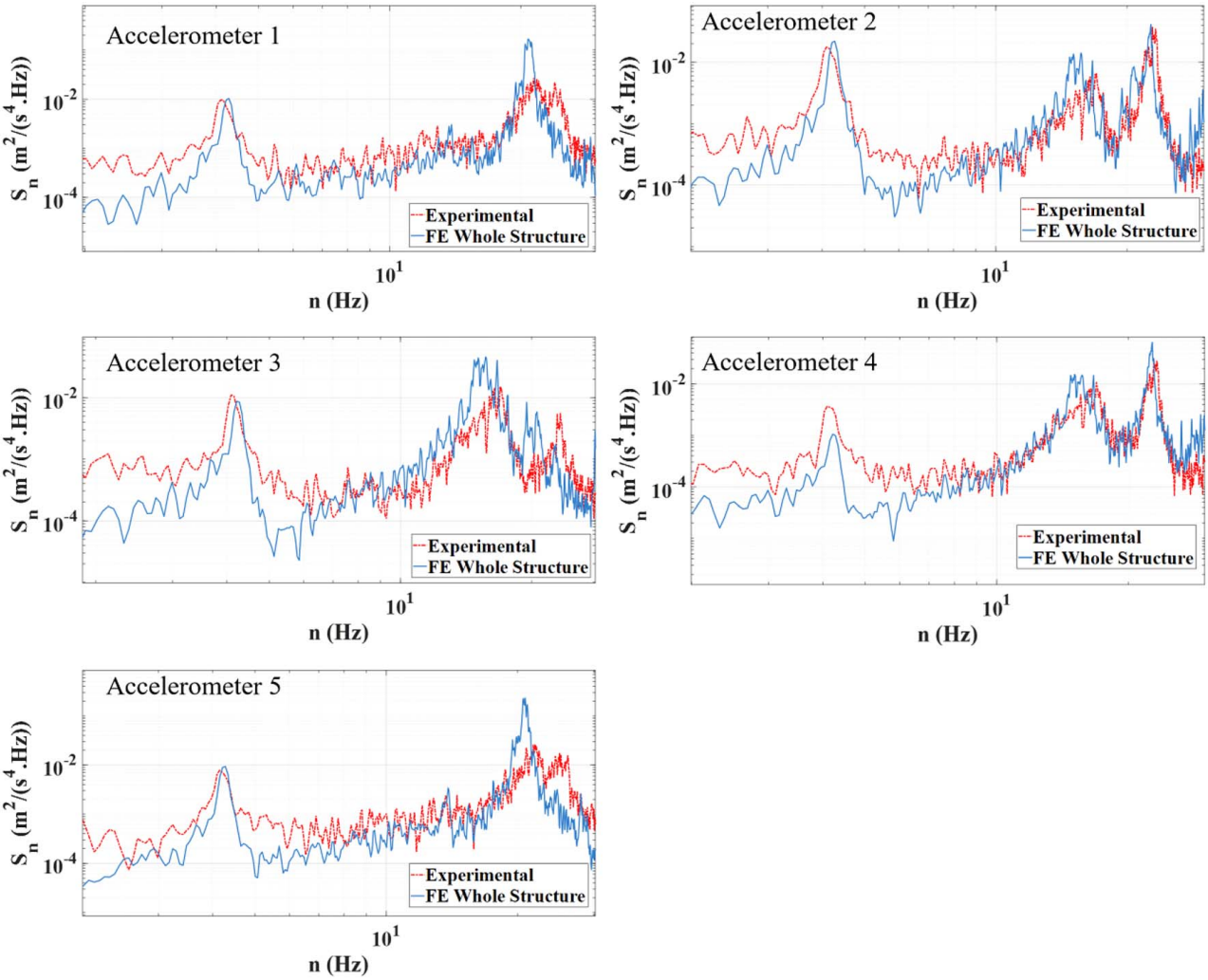

Fig. 23. Acceleration PSDs of the whole-structure FE model compared with the experiment data for 31.30 m/s and 0° wind.

For FE nodes not aligned with the pressure tap locations in the experiment, data are interpolated to compute the corresponding value for each node.

Calibration of the whole-structure FE model is conducted iteratively using the modeled wind load as input, adjusting the model parameters until the numerical model yields a dynamic response comparable with the experiment data. The FE model is deemed "comparable" when its root mean square (RMS) acceleration time history responses are within a 10% range compared with the experiment data. In this study, values associated with connections and structural silicones are adjusted. Fig. 18 highlights the locations of these connections and silicones adjusted in the whole-structure FE model. Table 5 summarizes the calibrated values for the connections and silicones. The process started with initial recommendations from literature on the mechanical properties of commercial structural silicone, including the study by Silvestru et al. (2018). The calibration involved iterative adjustments to these values, leading to the final calibrations that are specific to this study and differ from the initial recommendations. The specificity of the calibrated values is attributed to the specific FE modeling strategies employed, including the selection of element types and mesh density.

Table 7. RMS values of acceleration time history (m/s^2) of the whole-structure FE model compared with the experiment data for 40.23 m/s and 0° wind

Accelerometer #	FE analysis (m/s^2)	Experiment data (m/s^2)	Difference (%)
1	0.7108	0.8131	12.6
2	0.5265	0.5213	1.0
3	0.5449	0.4781	14.0
4	0.5358	0.4909	9.1
5	0.7267	0.8105	10.3

Fig. 19 presents the RMS of time history acceleration response of the calibrated whole-structure FE model compared with the experiment data, demonstrating a difference of less than 10% in all locations. Fig. 20 compares the acceleration responses in the frequency domain. A major frequency is apparent near 4 Hz in all five power spectral densities (PSDs), and other major frequencies are also clearly observed near 16 H and 24 Hz depending on the accelerometer locations. As shown in the figure, the whole-structure FE model reproduces the major frequencies observed in the experiment data with high fidelity.

The comparison of RMS values in time history strain response between the calibrated numerical model and the experiment data are shown in Fig. 21. The strain gauge 4 (S4) lacks

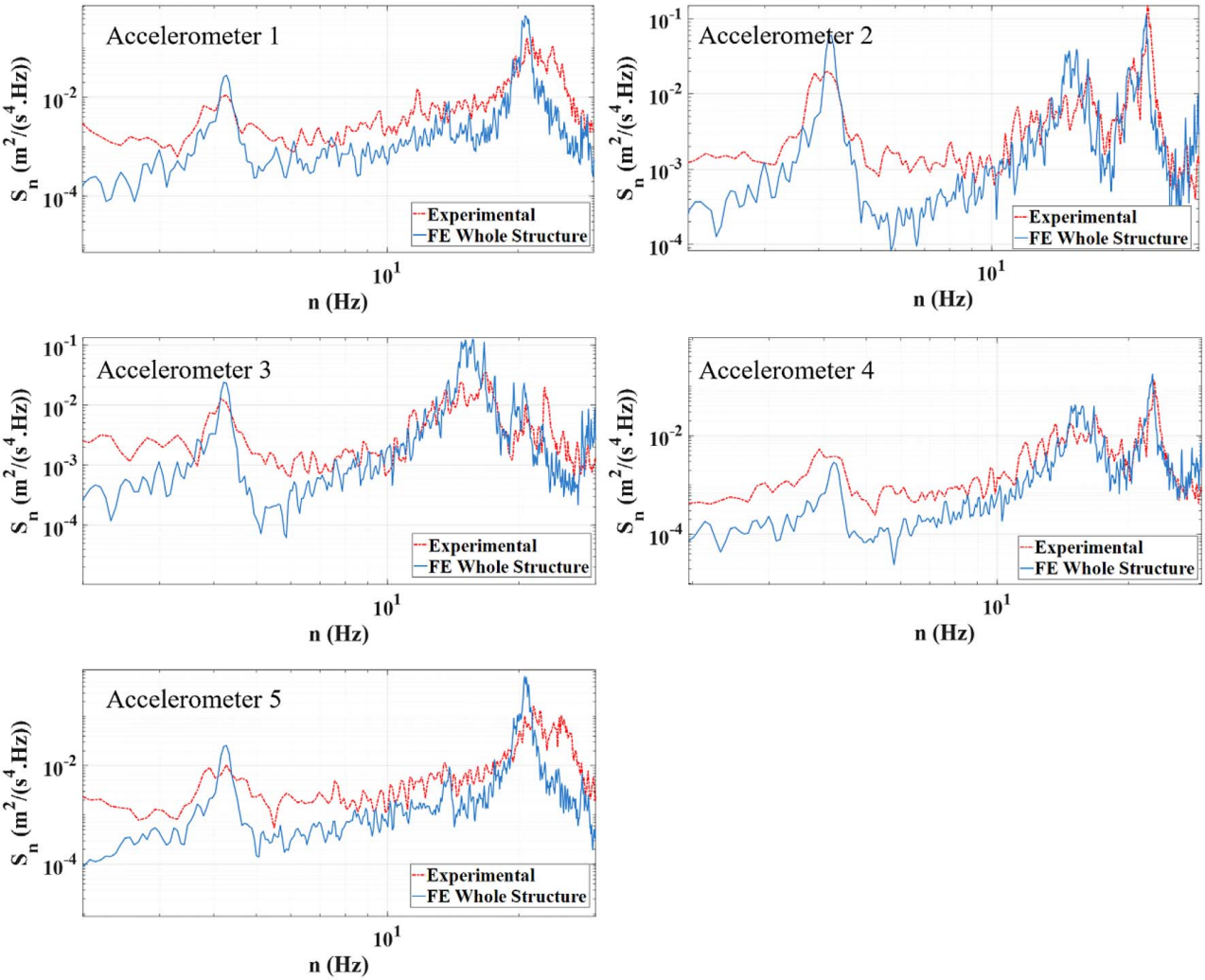

Fig. 24. Acceleration PSDs of the whole-structure FE model compared with the experiment data for 40.23 m/s and 0° wind.

data due to its malfunction, which was found after the experiment. The 10% criterion is also applied to strain time histories, achieving less than 10% difference for most locations. Exceptions include locations S5, S6, S8, and S9 in the center panels, where differences exceed 10%. The primary challenge arises from using 12-DOF beam elements to balance simulation fidelity and computational efficiency, given the complex geometries of the framing profiles. This leads to limitations in accurately representing the strain response on the mullion's extreme fiber, far from its neutral axis, since the strain gauges in the experiment are positioned on the extreme fiber of the mullion's cross section. Therefore, the differences exceeding 10% are observed near the center panels that experience more deformation. Employing 3D solid elements to model the framing profiles using, for example, 8-node hexahedral brick elements, could enhance the simulation accuracy. However, it would also significantly increase computational cost, making it less practical for the facade industry, since the modeling and analysis in the practice are typically performed using standard personal computers with limited computing power. Therefore, the study does not pursue further calibration of the strain response, acknowledging the limitations of using the beam elements. Nevertheless, the strain PSDs are reasonably comparable in the frequency domain, as shown in Fig. 22, including S5 and S8.

Table 8. RMS values of acceleration time history (m/s^2) of the whole-structure FE model compared with the experiment data for 40.23 m/s and 45° wind

Accelerometer #	FE analysis (m/s^2)	Experiment data (m/s^2)	Difference (%)
1	0.7101	0.7422	4.3
2	0.4415	0.4835	8.7
3	0.4106	0.4343	5.5
4	0.3962	0.4260	7.0
5	0.6617	0.6988	5.3

Analysis Results

Analysis of "Whole-Structure" FE Model

The calibrated whole-structure FE model is used to estimate the dynamic response under different wind loadings for model validation. Two different wind speeds, 31.30 and 40.23 m/s, and three different wind directions, 0°, 45°, and 90°, are considered to reproduce the wind-induced dynamic response. The C_p data obtained from

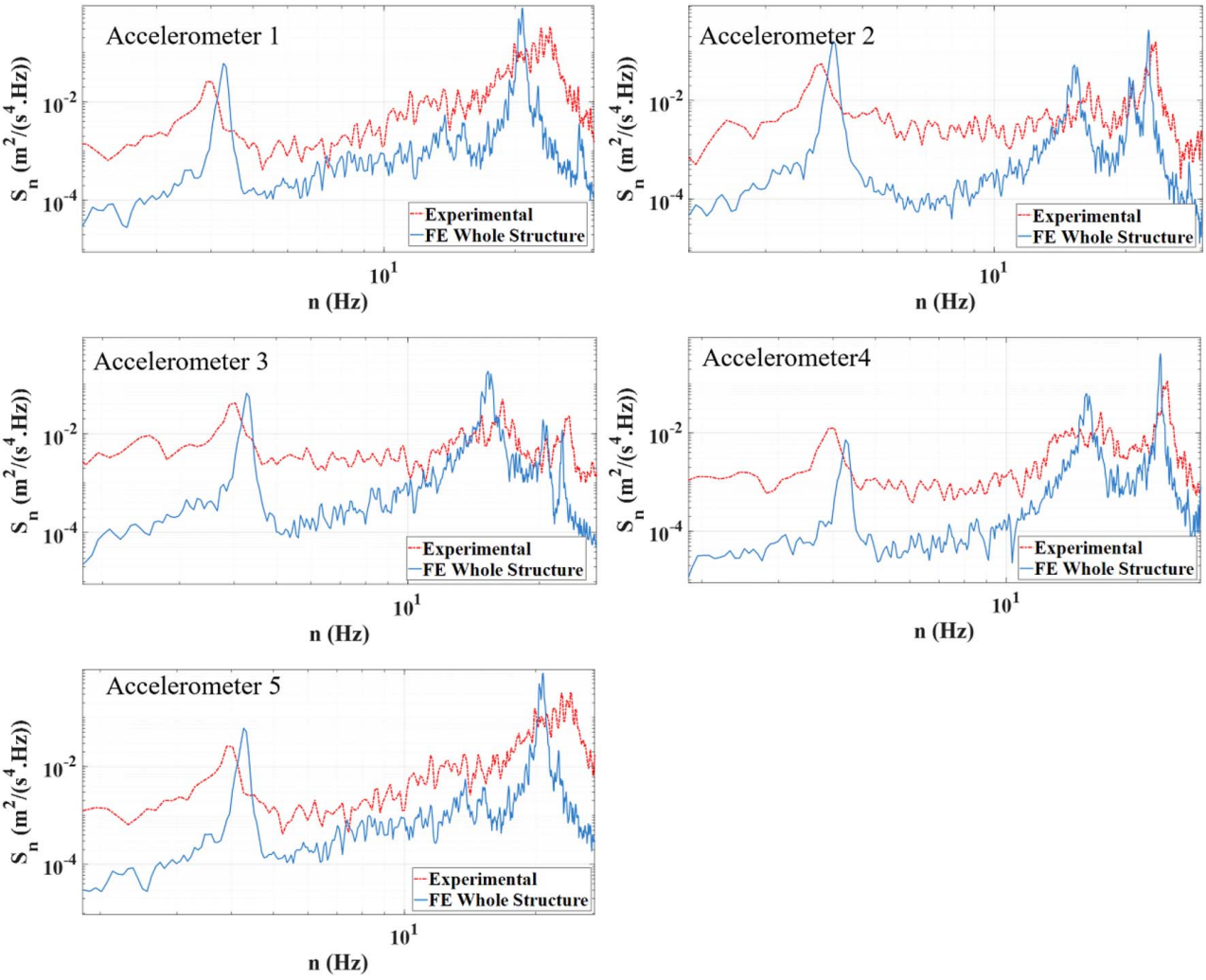

Fig. 25. Acceleration PSDs of the whole-structure FE model compared with the experiment data for 40.23 m/s and 45° wind.

the experiment are used to create the input nodal load time histories corresponding to each wind speed.

Table 6 presents the results for a 31.30 m/s and 0° direction wind. The results show a good comparison between the RMS values, with differences less than 13% between the FE model and the corresponding experimental data. In Fig. 23, the acceleration PSDs are plotted for all five locations, indicating that the numerical response realistically captures all major frequencies observed in the experiment data. The RMS values of acceleration response for 40.23 m/s and 0° direction wind are presented in Table 7, which also shows a good comparison between the numerical analysis and the experiment data with a difference up to a 14%. Fig. 24 shows the frequency domain response, which effectively captures the major frequencies. It is also important to note that the experimental data exhibit more energy, especially in the low-frequency band around the first natural frequency, compared with the numerical simulation results. The observed discrepancy in energy at the lower frequencies could be attributed to the inherent limitations of the simplified FE model, which adopts the beam elements to approximate the 3D frames, which could be better modeled with 3D solid elements while trading off the computational cost. Table 8 and Fig. 25 present the response for the wind at 40.23 m/s and 45° direction, and Table 9 and Fig. 26 show the results for 40.23 m/s wind at 90° crosswind direction. Although the numerical model is calibrated only for the normal direction wind, it demonstrates the comparable RMS values and captures the major frequencies for these different wind directions.

Table 9. RMS values of acceleration time history (m/s^2) of the whole-structure FE model compared with the experiment data for 40.23 m/s and 90° wind

Accelerometer #	FE analysis (m/s^2)	Experiment data (m/s^2)	Difference (%)
1	0.9355	1.0400	10.0
2	0.6582	0.5983	10.0
3	0.6086	0.5181	17.5
4	0.6294	0.5068	24.2
5	0.7879	0.8603	8.4

Analysis of "Facade-Only" FE Model

In the facade industry, it is common to model the facade without the building structure for numerical analysis. This practice is considered practical because modeling the entire system, including the building structure as well as the curtain walls, requires a significant effort. Therefore, the connection to the building structures is

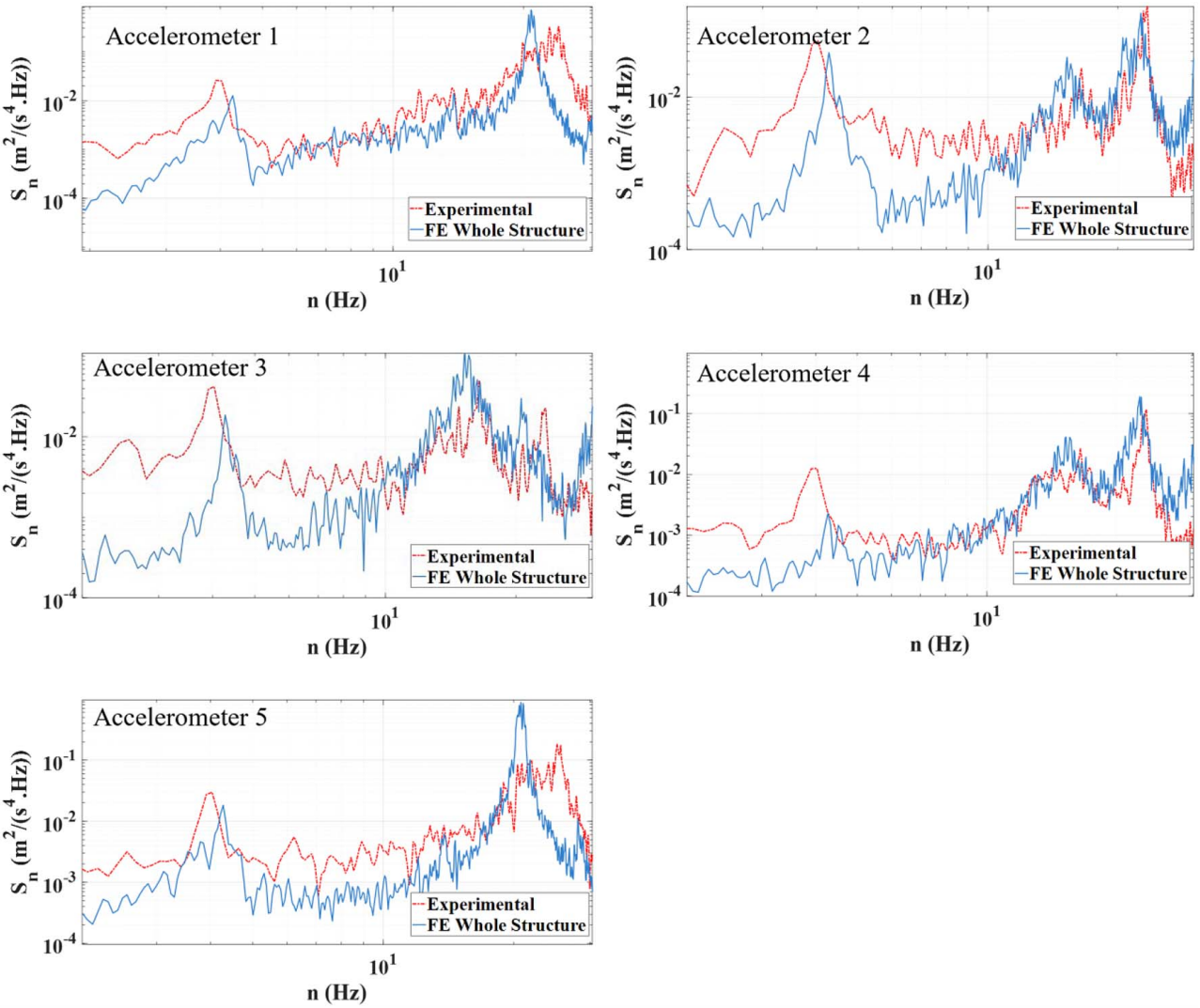

Fig. 26. Acceleration PSDs of the whole-structure FE model compared with the experiment data for 40.23 m/s and 90° wind.

typically modeled with a simplified boundary condition such as hinges or fixed ends. This practice, however, prompts questions regarding the potential differences in simulated dynamic behavior between numerical models that include the building structure and those that do not. This section addresses this issue by analyzing a "facade-only" model in comparison with the "whole-structure" model discussed in the previous sections. The "facade-only" model contains solely the single-skin curtain wall and is considered as a stand-alone system. The boundary condition of this model includes the connections to the supporting steel structure at both the

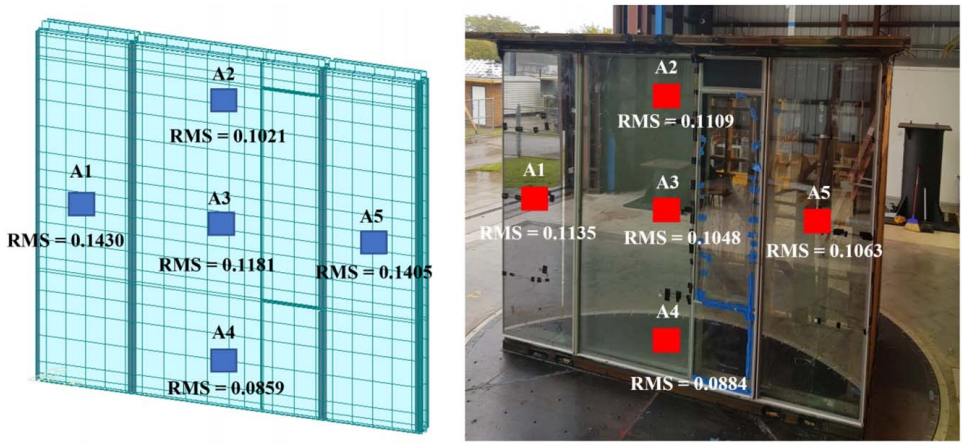

(a) (b)

Fig. 27. RMS values of acceleration time history (m/s^2) for 22.35 m/s and 0° wind: (a) facade-only FE model; and (b) experiment data.

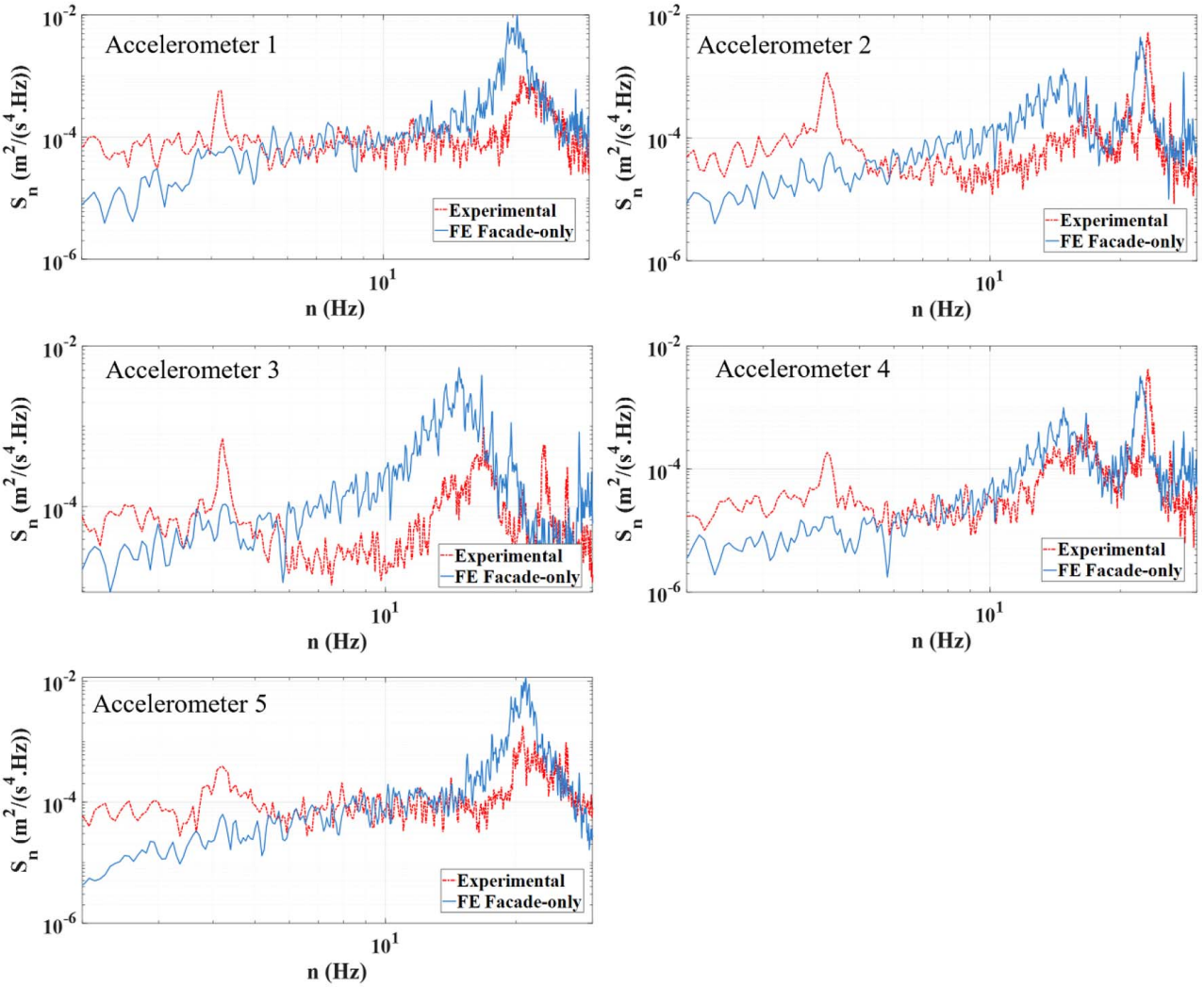

Fig. 28. Acceleration PSDs of the facade-only FE model compared with the experiment data for 22.35 m/s and 0° wind.

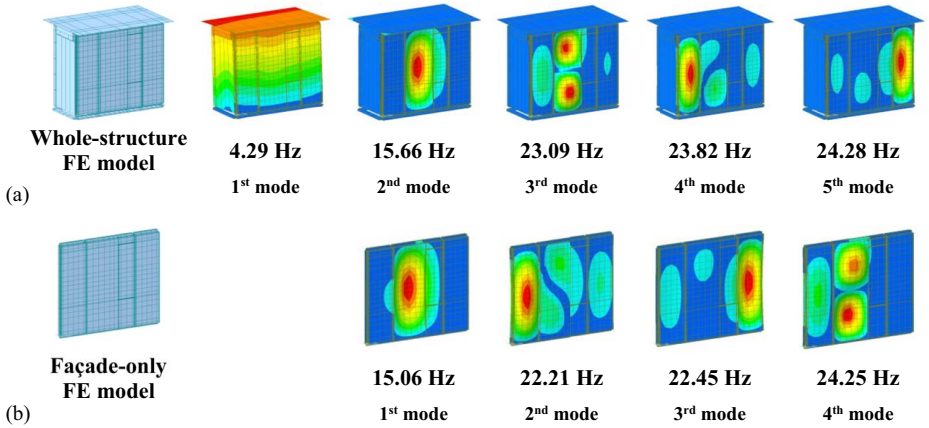

Fig. 29. Natural frequencies and mode shapes: (a) whole-structure FE model; and (b) facade-only FE model.

top and bottom, as depicted by the connections #1 and #2 shown in Fig. 18. A set of 6-DOF point springs are used for the boundary condition modeling, a strategy frequently adopted in the facade industry. The same values calibrated based on the experimental data for the whole-structure FE model are adopted for all modeling parameters. Figs. 27 and 28 present the simulation results of the facade-only model compared with the experiment data obtained for 22.35 m/s and 0° wind. The RMS values of acceleration response are comparable for the center panel while a major difference of more than 25% is shown in the side panels (A1 and

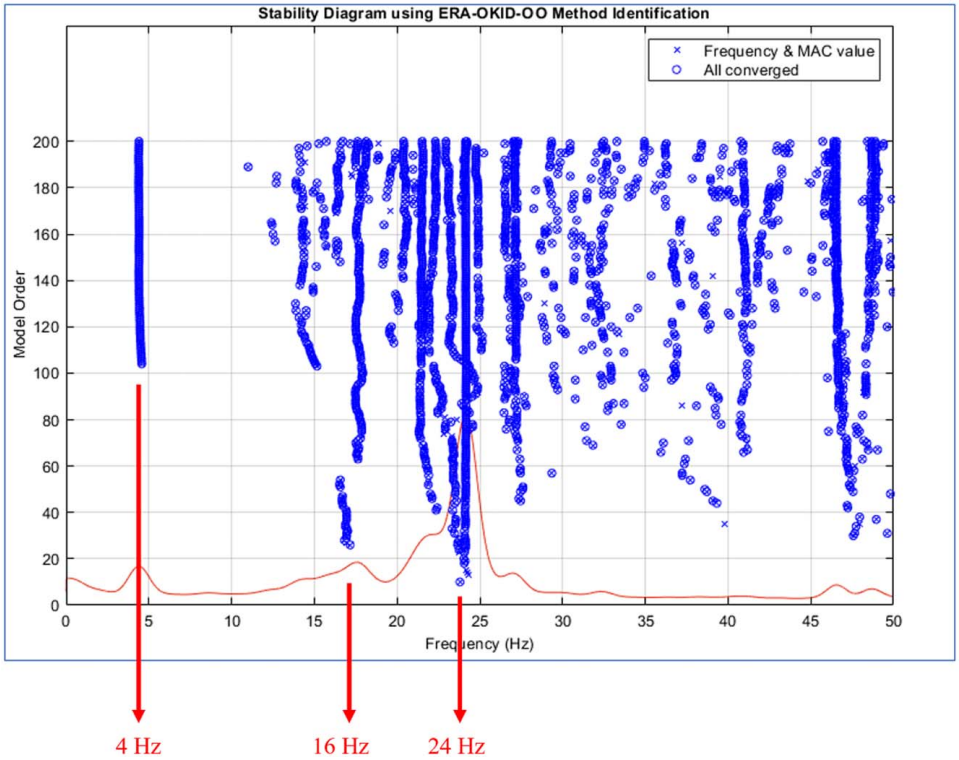

Fig. 30. Stability diagram created from the experimental acceleration data using the ERA-OKID-OO method.

A5). The difference is more remarkable for the PSDs in the frequency domain. In Fig. 28, a major frequency is clearly absent near 4 Hz.

Effect of Facade-Structure Interaction

Eigen analysis is conducted to further investigate the source of the difference between the facade-only model and the whole-structure FE model. The natural frequencies and mode shapes are shown in Fig. 29. Compared with the whole-structure FE model, the facade-only model completely lacks the first natural frequency around 4 Hz, although it still captures the other natural frequencies near 16 and 24 Hz. This observation can be translated that the natural frequency near 4 Hz originates from the interaction between the facade and its supporting building structure, while the higher natural frequencies are from the facade itself.

A system identification method is adopted to examine if the experimental data corroborates the same conclusion. To this end, the Eigensystem Realization Algorithm-Observer Kalman filter Identification-Output Only (ERA-OKID-OO) method by Chang and Pakzad (2014) is employed to generate a stabilization diagram of the experimental acceleration data. Fig. 30 shows the stability diagram, where a solid vertical line of stable poles is an indicator of a true mode of vibration, which is shown near 4, 16, and 24 Hz. These major frequencies are confirmed by the eigen analysis results obtained from the whole-structure FE model. However, the solid vertical line at 4 Hz is different from the lines at 16 and 24 Hz in

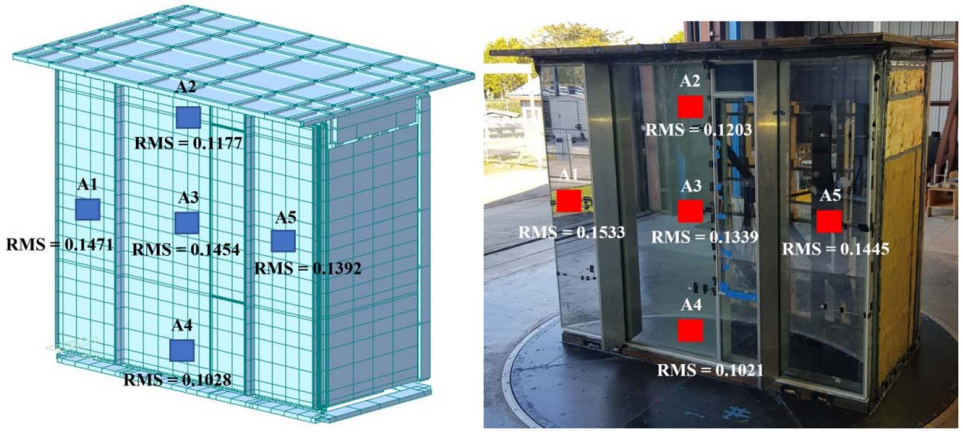

(a) (b)

Fig. 31. RMS values of acceleration time history (m/s^2) for 22.35 m/s and 0° wind: (a) whole-structure FE model with vertical protrusions; and (b) experiment data from wind tunnel test.

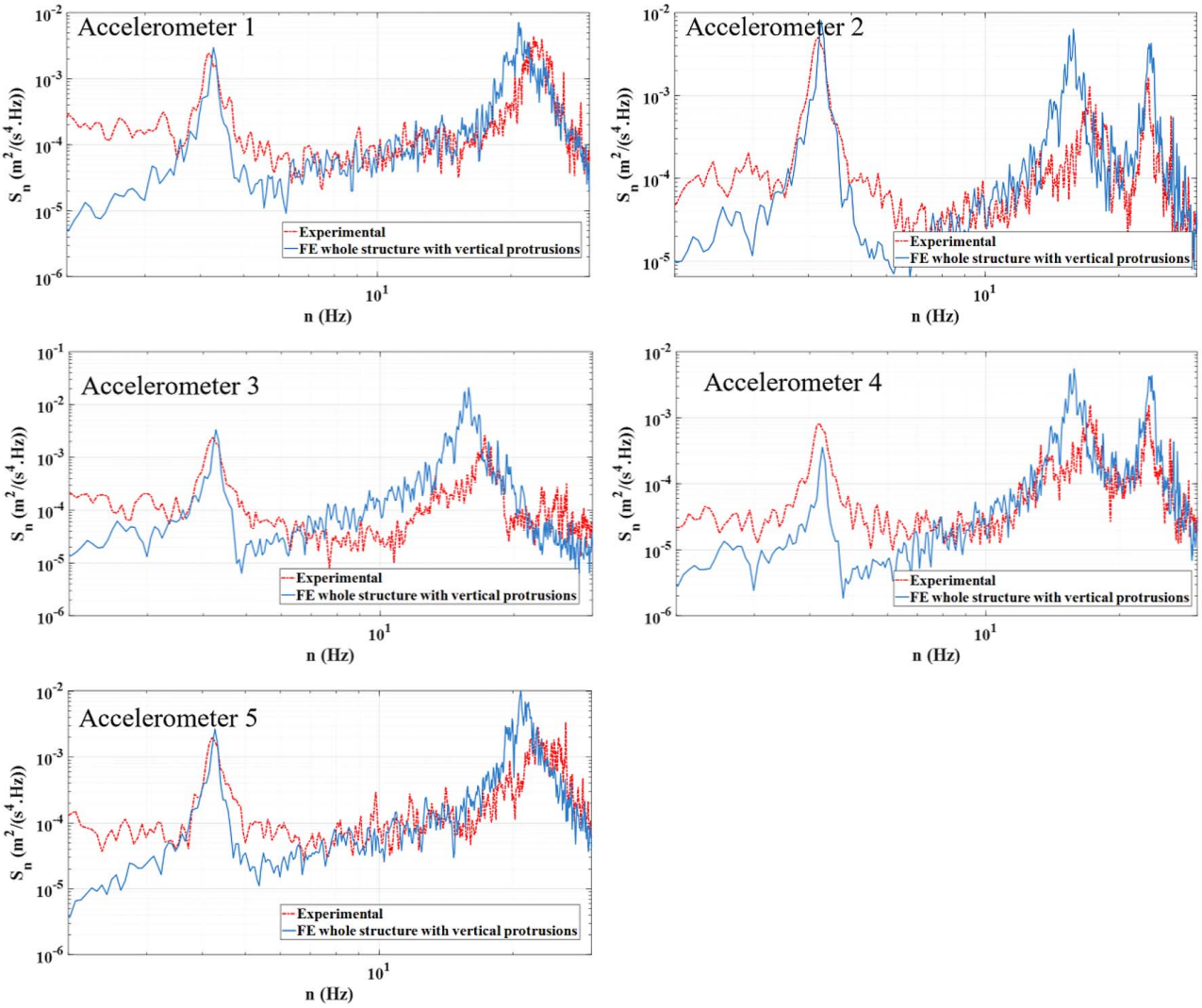

Fig. 32. Acceleration PSDs of the whole-structure model with vertical protrusions compared with the corresponding experiment data for 22.35 m/s and 0° wind.

the sense that the stable poles are realized for a much higher model order (above 100) while the stable poles at 16 and 24 Hz are realized at a lower order (as low as 20). The indication of a weak signal near 4 Hz highlights that the 4 Hz natural frequency is a result of the influence of the supporting structure. This is attributed to the fact that the sensors (accelerometers) are only mounted to the facade panels, which resulted in limitations in capturing the 4 Hz mode of the whole structure. On the other hand, the strong signals near 16 and 24 Hz indicate that these major frequencies are from the curtain wall itself. Therefore, it is evident that the facade-only FE model lacks the major frequency resulting from the interaction between the facade and the building structure. This absence can be seen as a limitation when only the facade is modeled.

Table 10. RMS values of acceleration time history at A3 of the whole-structure FE model, without and with vertical protrusions, compared with the experiment data for 22.35 m/s and 0° wind

Model	RMS acceleration (m/s^2)
FE analysis—without protrusion	0.1140
FE analysis—with protrusion	0.1454
Experiment data—without protrusion	0.1048
Experiment data—with protrusion	0.1339

Effect of Vertical Protrusion

The effect of vertical protrusion on the wind-induced dynamic response of the curtain-wall system is numerically investigated, with FE beam elements utilized to model the vertical protrusions. The modeled protrusions are connected to the mullions of the

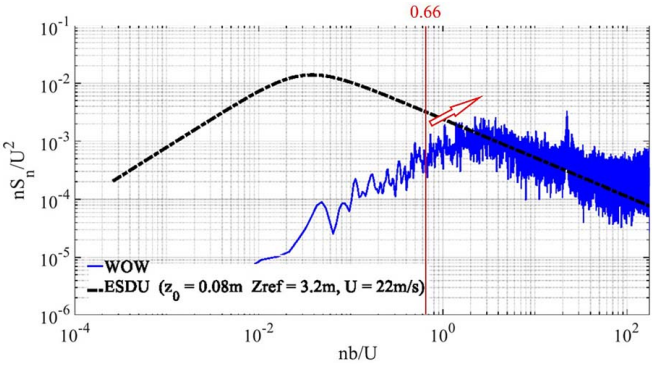

Fig. 33. Normalized wind turbulence power spectrum. (Modified from Alawode et al. 2023.)

whole-structure FE model using 6-DOF elastic links. Subsequently, the FE model with protrusions is subjected to 22.35 m/s and 0° wind to analyze its wind-induced dynamic behavior. Fig. 31 compares the RMS values of acceleration response, which demonstrates that the whole-structure FE model reasonably captures the dynamic behavior with vertical protrusions. The model also captures the major frequencies with high fidelity as shown in Fig. 32.

Compared with the curtain wall without the vertical protrusions, an increase in acceleration is observed with the installation of vertical protrusions. For example, as shown in Table 10, the RMS values of the acceleration response at A3 increase by more than 25%. The vertical protrusion adds stiffness to the system, thereby increasing the overall acceleration level. However, an increase in stiffness may not always result in an increased acceleration. Fig. 33 provides an additional explanation from the aerodynamic perspective. The figure depicts the normalized turbulence PSD obtained from the wind tunnel experiment, whereby the PSD is divided by U/b, where U represents the average wind speed measured at the roof height of the curtain wall, specifically 22 m/s, and b denotes the width of the curtain wall, which is 3.65 m. The whole-structure model has a fundamental natural frequency near 4 Hz, which is the first natural frequency. This corresponds to a value of 0.66 on this plot, and the frequency is positioned on the ascending side in the spectrum. Therefore, an increase in stiffness results in a higher natural frequency, which leads to an increase in the dynamic response. Given the first natural frequency of the curtain wall originates from the interaction between the facade and its supporting structure, the effect of vertical protrusion is influenced by the facade-structure interaction.

It is worth noting that the WOW EF wind simulation has a limitation in presenting low-frequency turbulence in large- and full-scale testing as shown in Fig. 33. This results in a noticeable deficiency in the low-frequency range of the PSD when compared with ESDU. The partial turbulence simulation (PTS) method, developed and validated in prior studies, can be used to effectively account for the absence of low-frequency components, providing a realistic estimation of peak pressure coefficients (Asghari Mooneghi et al. 2016; Moravej 2018). However, to allow for a direct comparison between experimental data and simulation results, this study does not apply the PTS method. The focus on the high-frequency part of the PSD is also of particular relevance to the analysis of curtain-wall systems in this study. Nevertheless, future research will explore the use of peak pressures after the PTS method to compensate for the low-frequency components.

Concluding Remarks

This study investigates the wind-induced dynamic behavior of a single-skin curtain wall using an FE facade model, which is developed based on the experiment data obtained from full-scale wind tunnel tests conducted at the NHERI WOW EF. A set of numerical modeling techniques are presented to realistically reproduce its wind-induced dynamic behavior. These techniques involve modeling the curtain-wall framing profiles with various cross sections, substituting DGU with equivalent glass, integrating the operable parts into the main curtain-wall frame, and creating connections among the frames and those between the frames and the glass. Two FE modeling approaches are employed to develop both "whole-structure" and "facade-only" models. The whole-structure model encompasses all elements present in the experimental test setup, including the supporting steel structure, sidewalls, and roof, as well as the curtain wall. In contrast, the facade-only model exclusively features the stand-alone curtain-wall system. The boundary condition in the facade-only model is simplified in a way that is commonly adopted within the facade design/engineering industry. These whole-structure and facade-only models are used to investigate the impact of facade-structure interaction on the wind-induced dynamic behavior of the curtain-wall system.

The whole-structure FE model is calibrated for a particular wind scenario with a speed of 22.35 m/s and 0° direction. It is demonstrated that the model can realistically reproduce the dynamic behavior in different scenarios involving various wind speeds and directions. Moreover, the FE model is also able to capture the major frequencies above 1 Hz in the response, mirroring what was observed in the wind tunnel experiment. Therefore, the FE modeling techniques presented in this study hold potential as a valuable tool for analysis and design in the facade industry. Furthermore, the findings of this study may prompt a re-evaluation of the ASCE 7 concerning the analysis and design of C&Cs, as the provisions currently do not require consideration of wind-induced dynamic effects on curtain-wall systems.

In contrast to the whole-structure FE model, the facade-only model completely lacks the first natural frequency originating from the interaction between the facade and its supporting structure. This result suggests that the interaction between the facade and building structure should be properly modeled to realistically simulate the wind-induced dynamic behavior of the facade. Furthermore, this hints that the facade's performance would change based on the structure it is mounted to. This study also investigates the effect of vertical protrusion on the facade's wind-induced dynamic behavior, demonstrating that the installation of a protrusion may change the facade's response with an increase in the curtain wall's overall stiffness. This suggests a potential increase in the amplitude of the dynamic response, which could lead to a higher probability of water ingress through the curtain wall. The effect of vertical protrusion is also influenced by the facade-structure's interaction. Ignoring the interaction between the facade and its supporting building structure could lead to an oversight of the wind-induced resonant response during the facade design phase. We encourage the research community to delve deeper into the complex phenomena related to the wind-induced dynamic behavior of curtain-wall systems, particularly focusing on the influence of the interaction between the facade and the building structure.

Data Availability Statement

Some or all data, models, or code that support the findings of this study are available from the corresponding author upon reasonable request.

Acknowledgments

This work is sponsored in part by the National Science Foundation under Grant No. IIP 1841503 and the I/UCRC Wind Hazard and Infrastructure Performance (WHIP) #2019-04 and #2020-04. The experiments in this project were conducted at the NHERI WOW EF (National Science Foundation Award No. 1520853 and No. 2037899). The authors are grateful to all laboratory staff at the WOW EF for the wind tunnel experiment. The authors also would like to thank the WHIP Industrial Advisory Board members for their comments and feedback. The authors would like to extend their appreciation to the Permasteelisa Group for providing the single-skin curtain-wall sample and its installation. The authors are grateful to Midas IT for providing a research license of

Midas Gen FEA software. The authors also express appreciation toward Dr. Minwoo Chang for the ERA-OKID-OO code used in this study. The financial aid provided by the Florida International University Graduate School through Doctoral Evidence Acquisition Fellowship and Dissertation Year Fellowship awarded to the first author of this paper is greatly appreciated. The opinions, findings, conclusions, or recommendations expressed in this article are solely those of the authors and do not represent the opinions of the funding agencies.

References

AAMA (American Architectural Manufacturers Association). 2005. *Standard test method for water intrusion of windows, curtain walls and doors using dynamic pressure*. Schaumburg, IL: AAMA.

Alawode, K. J. 2023. "Wind-induced vibration and wind-driven rain effects on curtain wall systems." Ph.D. dissertation, Dept. of Civil and Environmental Engineering, Florida International Univ.

Alawode, K. J., K. S. Vutukuru, A. Elawady, S. J. Lee, A. G. Chowdhury, and G. Lori. 2023. "Wind-induced vibration and wind-driven rain performance of a full-scale single-skin facade unit with vertical protrusions." *J. Archit. Eng.* 29 (2): 04023003. https://doi.org/10.1061/JAEIED.AEENG-1393.

ASCE. 2022. *Minimum design loads for building and other structures*. Reston, VA: ASCE.

Asghari Mooneghi, M., P. Irwin, and A. Gan Chowdhury. 2016. "Partial turbulence simulation method for predicting peak wind loads on small structures and building appurtenances." *J. Wind Eng. Ind. Aerodyn.* 157: 47–62. https://doi.org/10.1016/j.jweia.2016.08.003.

ASTM. 2021. *Standard test method for structural performance of exterior windows, doors, skylights and curtain walls by uniform static air pressure difference*. West Conshohocken, PA: ASTM.

Azzi, Z., F. Habte, K. S. Vutukuru, A. G. Chowdhury, and M. Moravej. 2020. "Effects of roof geometric details on aerodynamic performance of standing seam metal roofs." *Eng. Struct.* 225: 111303. https://doi.org/10.1016/j.engstruct.2020.111303.

Blain, C. A., et al. 2020. "The network coordination office of NHERI (Natural hazards engineering research infrastructure)." *Front. Built Environ.* 6: 108. https://doi.org/10.3389/fbuil.2020.00108.

Chang, M., and S. N. Pakzad. 2014. "Observer kalman filter identification for output-only systems using interactive structural modal identification toolsuite." *J. Bridge Eng.* 19 (5): 04014002. https://doi.org/10.1061/(ASCE)BE.1943-5592.0000530.

Chowdhury, A. G., I. Zisis, P. Irwin, G. Bitsuamlak, J. Pinelli, B. Hajra, and M. Moravej. 2017. "Large-scale experimentation using the 12-fan wall of wind to assess and mitigate hurricane wind and rain impacts on buildings and infrastructure systems." *J. Struct. Eng.* 143 (7): 04017053. https://doi.org/10.1061/(ASCE)ST.1943-541X.0001785.

ESDU (Engineering Sciences Data Unit). 2001. *Characteristics of the atmospheric boundary layer, Part II: Single point data for strong winds (neutral atmosphere)*. ESDU 85020. London: ESDU.

Estephan, J., A. G. Chowdhury, and P. Irwin. 2022. "A new experimental-numerical approach to estimate peak wind loads on roof-mounted photovoltaic systems by incorporating inflow turbulence and dynamic effects." *Eng. Struct.* 252 (1): 113739. https://doi.org/10.1016/j.engstruct.2021.113739.

European Committee for Standardization. 2000. *Curtain walling - Watertightness - Laboratory test under static pressure*. Eur. Stand. CEN/TC 33, (2000). EN 12155. Brussels, Belgium: CEN.

European Committee for Standardization. 2019. *Glass in building - Determination of the lateral load resistance of glass panes by calculation*. Eur. Stand. CEN/TC 129, (2019). EN 16612. Brussels, Belgium: CEN.

FEMA. 2005. *Hurricane charley in Florida: Observations, recommendations, and technical guidance*. FEMA 488. Washington, DC: FEMA.

Feng, C., A. Gan Chowdhury, A. Elawady, D. Chen, Z. Azzi, and K. S. Vutukuru. 2020. "Experimental assessment of wind loads on roof-to-wall connections for residential buildings." *Front. Built Environ.* 6: 10. https://doi.org/10.3389/fbuil.2020.00010.

Galuppi, L., and G. F. Royer-Carfagni. 2012. "Effective thickness of laminated glass beams: New expression via a variational approach." *Eng. Struct.* 38: 53–67. https://doi.org/10.1016/j.engstruct.2011.12.039.

Gerhardt, H. J., and F. Janser. 1994. "Wind loads on wind permeable facades." *J. Wind Eng. Ind. Aerodyn.* 53 (1–2): 37–48. https://doi.org/10.1016/0167-6105(94)90017-5.

Giusti, A. C. 2020. "Lake charles tower's window damage perplexes engineers." Engineering News-Record. https://www.enr.com/articles/50130-lake-charles-towers-window-damage-perplexes-engineers.

Habte, F., M. A. Mooneghi, A. G. Chowdhury, and P. Irwin. 2015. "Full-scale testing to evaluate the performance of standing seam metal roofs under simulated wind loading." *Eng. Struct.* 105: 231–248. https://doi.org/10.1016/j.engstruct.2015.10.006.

ICC (International Code Council). 2017. *Testing application standard (TAS) 202-94 criteria for testing impact and nonimpact resistant building envelope components using uniform static air pressure*. Washington, DC: ICC.

Irwin, P., K. R. Cooper, and R. Girard. 1979. "Correction of distortion effects caused by tubing systems in measurements of fluctuating pressures." *J. Wind Eng. Ind. Aerodyn.* 5 (1–2): 93–107. https://doi.org/10.1016/0167-6105(79)90026-6.

Memari, A. M., N. Simmons, and R. L. Solnosky. 2021. "Developing FEM procedures for four-sided structural sealant glazing curtain wall systems with reentrant corners." *Buildings* 11 (12): 597. https://doi.org/10.3390/buildings11120597.

MIDAS IT (Midas Information Technology). 2021. *Midas Gen software*. Seongnam-si, Gyeonggi-do, South Korea: MIDAS IT.

Moravej, M. 2018. "Investigating scale effects on analytical methods of predicting peak wind loads on buildings." FIU Electronic theses and dissertations, Dept. of Civil and Environmental Engineering, Florida International Univ.

Moravej, M., A. Chowdhury, P. Irwin, I. Zisis, and G. Bitsuamlak. 2015. "Dynamic effects of wind loading on photovoltaic systems." In *14th Int. Conf. on Wind Engineering*, 1–133. Porto Alegre, Brazil: ICWE.

Nakagami, Y. 2003. "Probabilistic dynamics of wind excitation on glass facade." Doctoral dissertation, Dept. of Civil and Environmental Engineering Sciences, Technical Univ. of Darmstadt.

NCEI (National Centers for Environmental Information). 2022. U.*S.* b*illion-dollar* w*eather and* c*limate* d*isasters (2022)*. Asheville, NC: NCEI.

NSB (National Science Board). 2007. *HURRICANE WARNING: The critical need for a national hurricane research initiative*. Arlington, VA: NSB.

Pariafsai, F. 2016. "A review of design considerations in glass buildings." *Front. Archit. Res.* 5 (2): 171–193. https://doi.org/10.1016/j.foar.2016.01.006.

Rizzo, F., A. Franco, A. Bonati, G. Maddaloni, N. Caterino, and A. Occhiuzzi. 2021. "Predictive analyses for aerodynamic investigation of curtain walls." *Structures* 29: 1059–1077. https://doi.org/10.1016/j.istruc.2020.11.077.

Sakhnovsky, A. A. 1991. *Full-scale performance testing of curtain walls*. West Conshohocken, PA: ASTM.

Sanders, R. M., and C. A. Hargrove. 2012. "Preventing and treating failure in glazed curtain wall systems." *J. Archit. Eng.* 29 (2): 1–8.

Silvestru, V. A., O. Englhardt, and J. Schneider. 2018. "Investigations on linear silicone joints for glass-metal elements with composite structural behavior." In *Conf. on Architectural and Structural Applications of Glass*. Delft, Netherlands: Delft Univ. of Technology.

Vutukuru, K. S., K. J. Alawode, A. Bakhtiari, A. Elawady, S. J. Lee, A. G. Chowdhury, and G. Lori. 2021. "Full-scale experimental testing to investigate wind-induced vibrations on curtain wall systems." In *Proc., Int. Structural Engineering and Construction*. Cairo, Egypt: ISEC Press.

Yu, Y., T. Liu, Q. Zhang, and B. Yang. 2017. "Wind-induced response of an L-shaped cable support glass curtain wall." *Shock Vib.* 2017: 1–16. https://doi.org/10.1155/2017/4163045.